A TORSION PENDULUM INVESTIGATION OF TRANSIENT MACHIAN EFFECTS

A Thesis

Presented to the

Faculty of

California State University, Fullerton

In Partial Fulfillment

of the Requirements for the Degree

Master of Science

in

Physics

By

Thomas Louis Mahood

Approved by:

James F. Woodward, Committee Chair
Departments of History and Physics

11/11/99
Date

Stephen W. Goode
Stephen Goode, Member
Department of Mathematics

11/11/99
Date

Ronald Crowley, Member
Department of Physics (Emeritus)

11/11/99
Date

Abstract

Mach's Principle proposes inertia is gravitationally induced by all matter in the universe. Recent theory suggests the possibility of transiently altering the inertial rest mass of an object by means of carefully applied acceleratory motion. When combined with application of an external force, theory suggests a net force may be extracted, manifesting as a form of "propellantless propulsion". This theory is subjected to experimental test with two differently designed test devices, utilizing a sensitive torsion arm pendulum within an evacuated chamber. Both devices utilized stacks of piezoelectric discs, driven by carefully phased and mixed oscillating power signals, inducing bulk accelerations within the piezoelectric material. After validation procedures, small amounts of motion were definitely observed, consistent with a force being generated by the test devices on the order of $3x10^{-2}$ dynes, with input power around 100 watts. However, this is far smaller than predicted and the discrepancy likely results from oversimplification of the theory.

Acknowledgements

I'd like to thank Dr. James Woodward for turning what should have been an ordinary Masters degree into quite an adventure. I'd also like to express my thanks to my wife Jeri, who through her support made it possible for me to spend my time chasing new dragons. Half the degree is hers.

Table of Contents

List of Illustrations

Figure Page

List of Tables

Table Page

I. Introduction

In the past few years, some truly remarkable new concepts and theories have been presented regarding exotic forms of propulsion for future space vehicles. What was once considered the realm of science fiction is now being actively debated in numerous scientific journals throughout the world. Topics like wormholes, “warp bubbles”, superluminal transport, zero point energy and various schemes of “propellantless propulsion” have stimulated a great deal of discussion and thought. Serious researchers and theorists have moved in, evicting the crackpots, with the sense there just may be something to some of these things. Sessions on some of these topics have become part of many mainstream conferences held by the aerospace community, and NASA is actively promoting research in these areas. Certainly the scientific payoff of any of them warrants at least a modest investigation. This paper will examine one such possibility: that of propellantless propulsion by the induction of transient mass shifts. While propellantless propulsion is certainly a worthwhile motivation, it is worth mentioning that the experimental work involved in this investigation is also a purely scientific examination of the validity of “Mach’s principle”: the proposition that inertial reaction forces are produced by the gravitational interaction of local objects with chiefly the most distant matter in the universe.

In essence, this paper will attempt to answer the question, “Is there anything to this?” and is primarily an experimental investigation. However a digression into the basic theory under examination is necessary in order to put the experimental effort in its proper context. The following is a simplified and brief overview. A formal derivation of the transient mass fluctuation effect upon which this is based may be found in (Woodward, 1996), and a thorough, detailed mathematical derivation from first principles that elaborates several matters not done explicitly by Woodward is contained in the Appendix. A complete theoretical presentation regarding the causation of inertia may be found in Woodward and Mahood (1999).

Theoretical overview

General Relativity Theory (GRT) with certain boundary conditions holds to be true that the inertia of an object is caused by the interaction of that object with the gravitational effects of all the rest of the matter in the universe. This has been known for many years as "Mach's Principle". In many circumstances this interaction with distant matter can be characterized by a simple scalar potential. Fluctuations in this universal

gravitational potential, caused by making massive objects accelerate, propagate at the speed of light.

It is also a prediction of the theory under investigation here, that by subjecting a test mass to a time-varying acceleration and deceleration, the mass gets slightly "out of phase" with the gravitational potential, and as a result its inertial mass very briefly gets a bit smaller and larger, just as small time delays that occur in electromagnetic radiation reaction situations lead to transiently unbalanced forces. Specifically the theory predicts (Eq. A.20 of the Appendix, reproduced here) that:

$$\nabla^2 f - \frac{1}{c^2}\frac{\partial^2 f}{\partial t^2} \approx 4\pi G \rho_0 + \frac{f}{\rho_0 c^2}\frac{\partial^2 \rho_0}{\partial t^2} \tag{1}$$

Where f is the gravitational potential, c is the speed of light, G is the Newtonian constant of gravitation and ρ_0 is the proper rest density of the test mass. This basic field equation is a relativistically invariant generalization of Newtonian gravity. As is apparent, the normal Newtonian source term now accompanied by an interesting transient term.

To further clarify the transient effect happening here, Eq. 1 may be rearranged (Eq. A.21 of the Appendix, reproduced here) to give:

$$\nabla^2 f - \frac{1}{c^2}\frac{\partial^2 f}{\partial t^2} \approx 4\pi G\left(\rho_0 + \frac{f}{4\pi G \rho_0 c^2}\frac{\partial^2 \rho_0}{\partial t^2} \right), \tag{2}$$

It now becomes obvious that the time-varying, transient term must act as an "adjustment" to the proper mass density of the source, based upon the second derivative of the time rate of change in the test mass's proper density, which is either added to or subtracted from the proper density depending upon the instantaneous value of the second time derivative.

If the applied force and the resulting acceleration are periodic, then over any given period of time, these mass increases and decreases will normally average out to zero and won't be apparent unless special measures are taken. Because the mass shift effect is a non-linear result of time-varying acceleration, careful selection of acceleration and deceleration profiles can yield a situation where the mass of a test object is slightly reduced during its acceleration phase, and slightly increased during its deceleration phase (or vice versa).

If the object experiencing the transient mass shifts is pushed by another outside force as it gets heavier, and then pulled by this force as it gets lighter, a net reaction force on the external pushing agent may be extracted. An example of this is shown in Figure 1.

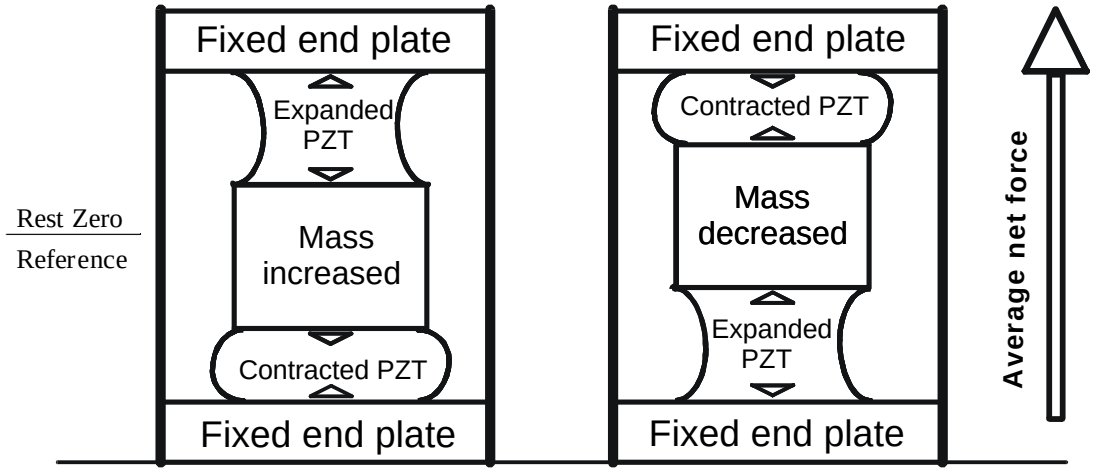

Figure 1. Net force extraction from transient mass shifts. An example of how a net force may be extracted if transient mass shifts are possible. A test mass, capable of transient mass increases and decreases is shuttled by two phase-reversed PZT stacks between two fixed end plates.

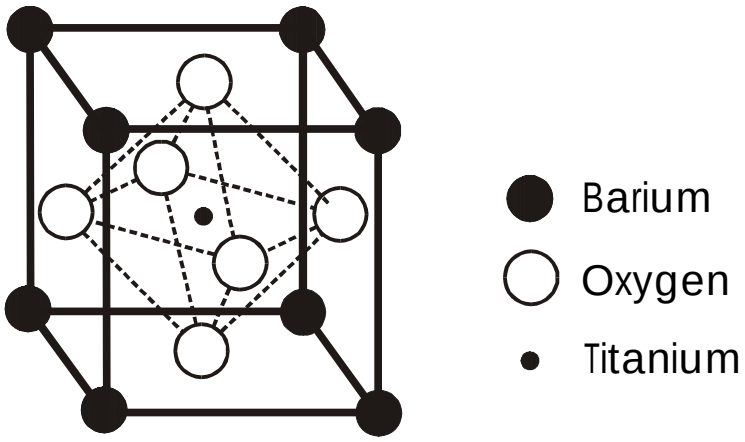

Figure 2. Unit cell of Barium Titanate. When subjected to an electric field the central titanium ion experiences substantial movement. Through the use of an oscillating electric field, it may be rapidly shuttled.

An object capable of transient mass shifts is placed between two piezoelectric transducers, with one transducer operating in reverse of the other (i.e., as one expands, the other contracts at the same rate). The left portion of Figure 1 shows that as the object gets heavier, the PZT transducers move it downward. Then, as the object gets lighter, depicted on the right side of Figure1, the transducers move it upward. It is obvious that if such actions could in fact be accomplished, a net upward force would result.

At this point any reasonable person considering such a fantastical scheme should immediately object that devices based upon it clearly violate conservation of momentum and energy laws, and therefore can't possibly work. At first glance, such concerns are perfectly understandable. But since the derivation of the transient mass effect comes from a straightforward relativistic generalization of Newton's second law, one can justifiably demand all momentum within an isolated system must balance. The trick here is determining what constitutes the isolated system these devices operate in. Since the inertial force presumably arises from all other matter in the universe (a very "non-local" interaction), manipulations of this inertial force must induce reactions in its source, that is, the rest of the universal matter. The boundaries of the system under consideration must be drawn to include all interacting components. Since these effects appear instantaneous, it presupposes the momentum transfer is accomplished via advanced and retarded gravitational wave disturbances propagating at the speed of light between the devices and all matter in the universe. Given this scenario, conservation of momentum is arguably not violated, despite superficial appearances.

A major issue to resolve is how best to subject an object to the large, varying accelerations needed to see this predicted effect. Initial experimentation in this area focused on generating accelerations within capacitor dielectric material (Woodward 1992 and 1996).

Most high energy density capacitors utilize some form of barium titanate compound as their dielectric material. Barium titanate falls into a class of materials known as perovskites, which at the molecular level reveal a highly structured crystalline lattice arrangement, usually of cubic configuration (Moulson and Herbert 1990). A typical unit cell of barium titanate, shown in Figure 2, consists of a cube with eight barium ions on the outer corners, an inner octahedral structure of six oxygen ions, and a central titanium ion. When subjected to an electric field, the entire structure displaces in response (i.e., polarizes), while retaining its general shape. The titanium ion experiences by far the largest displacement, and when subjected to an oscillating electric field, can be made to shuttle rapidly back and forth. Thus by applying a rapidly varying voltage to a capacitor, some of the atomic constituents of the capacitor’s dielectric can be subjected to substantial accelerations, much larger than could be accomplished by bulk mechanically vibrating an object.

According to the theoretical derivation of the effect, if a capacitor is charged and discharged by a sine wave, some portions of its dielectric will experience two mass

increases and two mass decreases per charging cycle (e.g., there are two times when the dielectric material accelerates and two times when it decelerates in each cycle). If the capacitor is then firmly attached to a properly timed piezoelectric transducer (PZT) moving the capacitor back and forth at twice the frequency the capacitor is being driven at, a net force may be produced. This occurs because the capacitor is slightly lighter when the transducer pushes it, and slightly heavier when the transducer pulls it and thus does not average out to zero as explained above. In mathematical terms, if one sinusoid (a mass shift) is multiplied by a second sinusoid (an external force), the result is not zero, but is in fact a DC offset. Specific details, as well as the mechanism by which this occurs, is contained in the Appendix, particularly from Eqs. A.27 through A.32.

Proceeding in this manner, a simplified, linearized prediction of average force (Eq. A.34 of the Appendix, reproduced here) may be obtained:

$$< \mathrm{F} > = -\frac{w^3 d\, l_0 \mathrm{P}}{p\, G\, r_0 c^2} \tag{3}$$

where w is the frequency the capacitor is cycled at, $d\, l_0$ is the excursion the capacitor is subjected to and P is the RMS value of the power delivered to the capacitor in watts

This concept of shuttling a capacitor while subjecting it to a sinusoidal driving voltage was used in a number of early experiments, and yielded positive results (Woodward 1996). However the necessity of having an extremely positive mechanical coupling between the PZT and the capacitor proved problematic, so other methods were examined.

It was discovered that PZT material itself was a superior replacement for the capacitor dielectric. This shouldn't be too surprising, as the materials are quite similar. The main difference is that in most quality capacitors, the electromechanical response (i.e., the dielectric's piezoelectric response) is suppressed to the extent possible by the addition of small amounts of impurities to the barium titanate. However piezoelectric transducers are quite the opposite, with their electromechanical response engineered to be as large and refined as possible. Thus much more total atomic motion can obtained from piezoelectric material than from capacitors, all other things being equal, since in addition to the motion induced by polarization of the material, it also undergoes bulk motion.

It was further found that discrete shuttling and mass-shift components were not necessary. Rather than creating a transient mass shift in one component as it is shuttled by another component, it was possible to combine both actions in a single unit. This was accomplished by driving a piece of piezoelectric material with two signals at once. A large amplitude sine wave is mixed with a lower amplitude sine wave of double the frequency of the first, at an appropriate phase offset, and applied to a PZT. Due to the principle of superposition, the action is the same as if the PZT was being driven by two

separate signals. The results proved to be much larger than those obtained for shuttling a separate capacitor, construction was greatly simplified and reliability increased.

It is this concept, driving piezoelectric material with mixed sine waves to produce a net force, that is the focus of this experimental investigation.

II. Previous Work in This Area

This is an area little explored to date by other researchers. The published experimental reports outstanding are almost exclusively those issued by James F. Woodward of California State University, Fullerton. Although Woodward has published several reports on experimental results (as well as papers covering theory), the most exhaustive experimental paper by far is *A Laboratory Test of Mach's Principle and Strong-Field Relativistic Gravity* (Woodward 1996).

In this paper, Woodward reports positive results obtained by shuttling a ring of six high energy density capacitors, mounted atop a stack of piezoelectric discs. Force measurements were made utilizing a high precision Hall effect force transducer, which in effect acted as an extremely sensitive weight scale with a rapid response rate. Woodward described force levels of a few dynes at an operating frequency of 11 KHz.

While Woodward's work is quite clear and specific in regard to this effect, there is published work by another that is at least suggestive of the effect's existence. In the late 1980's, Phillips Laboratory (of the Propulsion Directorate, a subdivision of the Air Force Systems Command), contracted with Veritay Technology of East Amherst, New York for an investigation into what has been called the "Biefield-Brown effect" (Talley 1991). The Biefield-Brown effect dates back to the 1920s, and claims that shaped, fixed electrodes, separated by dielectric material and charged with a high DC electrical potential, will exhibit a propulsive force. This particular investigation utilized a torsion pendulum within a chamber evacuated to levels of 10^{-6} torr, and had a force measurement threshold of 0.002 ìN. Talley's apparatus is shown in Figure 3. Overall, the report indicates a very high level of care and rigor went into the experimental protocols. The final report of the investigation, authored by Robert L. Talley, concluded that no such Biefield-Brown propulsive effect was occurring, at least to the voltage potentials utilized by the experimenters.

However during the testing, Talley observed what he termed "an anomalous force" during conditions of electrical breakdown of the dielectric. The force, while small, could not be attributed to any apparent error in the experimental apparatus, and remained unexplained by Talley.

This "anomalous force" appeared in two specific situations. First, during experimentation with 600 Hz pulsed fields at 19 kV, a very weak force was detected just above the noise level of the apparatus. But because it was close to the experiment's noise level, it was noted and dismissed.

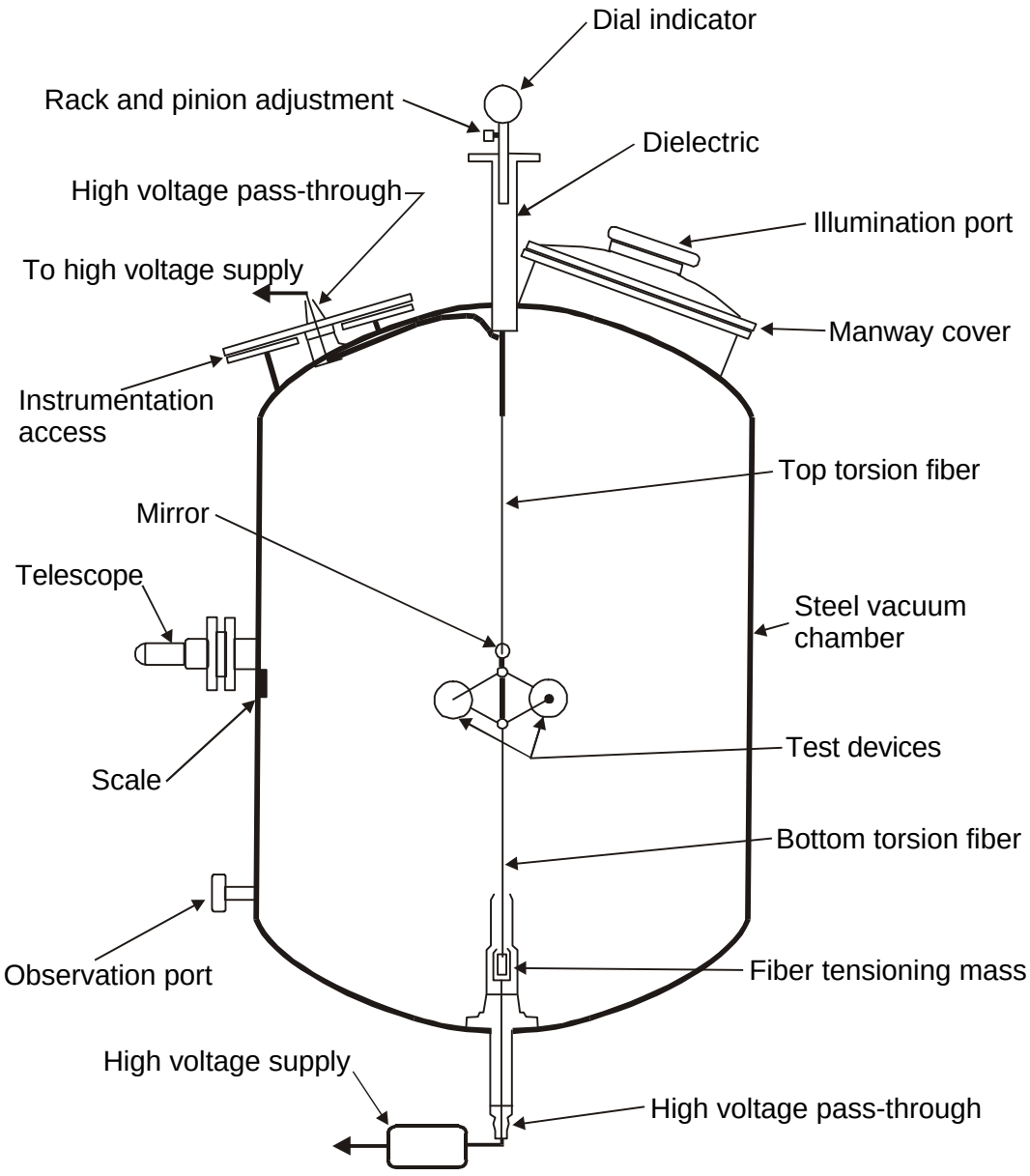

Figure 3. Talley's 1991 experimental apparatus, excluding vacuum and electronic support systems (From Talley 1991).

In later testing, a larger force was apparently detected. This occurred in a configuration in which the electrodes were separated by a cylindrical piece of piezoelectric material (lead titanate-lead zirconate) 0.635 cm in diameter and 1.61 cm in length, shown in Figure 4. When the DC potential was raised to the vicinity of 19 kV, a random pulsing breakdown across the dielectric began, and the torsion arm underwent rotation. When the voltage was reduced to 15 kV, pulsing ceased and the arm returned to its initial position. What is intriguing about this behavior is that when the piezoelectric material was replaced by an identical dielectric made of acrylic in a subsequent test, similar breakdown occurred, but no motion of the torsion arm was observed. This at least suggests the possibility that under conditions of rapidly varying potential, and accompanying electromechanical activity, piezoelectric material exhibits some rather interesting behavior.

Although in its conclusions the report recommended this anomalous force be investigated further, my inquiries reveal that this recommendation was apparently never followed. Upon reflection it is likely the conditions of breakdown in Talley's apparatus inadvertently mimic the application of mixed waveform signals to the titanate dielectric and as a result one might well expect to see the forces produced if transient mass fluctuations do indeed occur.

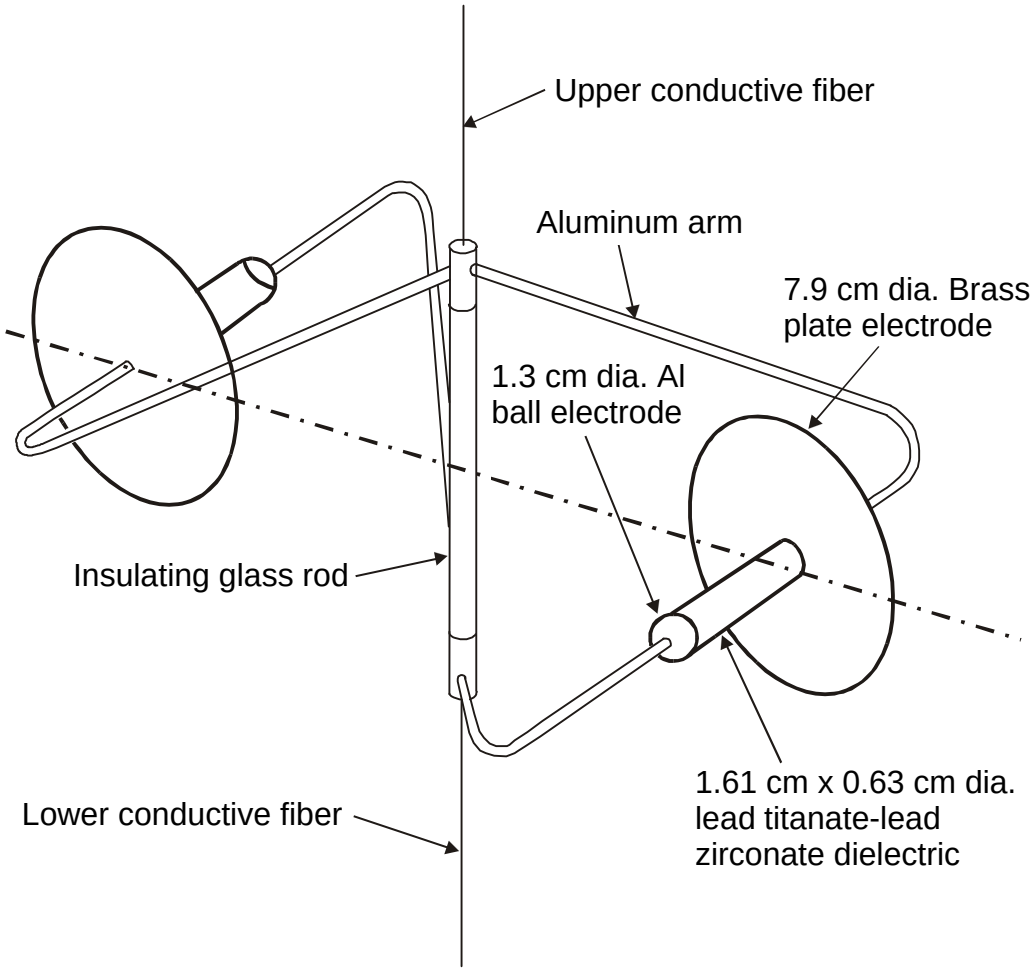

Figure 4. Talley's torsion arm configuration utilizing ball and disc electrodes, separated by a cylindrical lead titanate-lead zirconate dielectrics (From Talley 1991).

III. Experimental Apparatus and Configuration

To get high sensitivity and operational simplicity while still keeping the apparatus within reasonable fabrication means, a torsion pendulum design was selected as the method of force measurement. Since the candidate test units required a source of power, a dual fiber torsion pendulum (i.e., a suspension consisting of a fiber above the torsion arm and a fiber below) seemed ideal, as the fibers could be metallic and also serve as power feeds (as in Talley's system). Unfortunately, this eventually turned out to be the source of a number of difficulties with the device that had to be overcome. Due to the possibility of spurious ultrasonic effects created by the operation of test devices in the air, it was necessary to encase the pendulum within a vacuum chamber. Test devices were mounted at each end of the torsion arm and deflections of the torsion arm were measured by the movement of a laser beam, reflected off a mirror on the torsion arm, onto a scale outside the chamber.

The overall layout of the electronics for the experimental setup is shown in Figure 5. The signal generator and mixer created two sine waves, one at twice the frequency of the other, and mixed them together at some chosen phase offset. This output signal was then switched on and off by a personal computer running timing software written for that purpose. The monitored signal, at a level of about 1.5 volts, was next fed into a Carvin HT-1000 stereo amplifier (a 1,000 watt professional grade unit) boosting the voltage amplitude to around 70 volts. The output of the amplifier was fed through a heatsinked block of power resistors totaling 4 ohms (for impedance matching to the amplifier's output), and then into the primary winding of a 1:5 toroidal step-up transformer. While it may be a little unusual to do impedance matching on the primary side of a step-up transformer, it was found this allowed use over a far wider range of frequencies and secondary reactances than were the matching done on the secondary side. The output of the transformer was passed through a low-value series resistor for current measurement, and a voltage divider for voltage measurement. Besides the voltage and current waveforms being monitored on oscilloscopes, the values were fed into a power meter, which computed the instantaneous power. Both the instantaneous and averaged rectified power could be displayed. The signal was finally sent to the test chamber and test units in the evacuated test chamber.

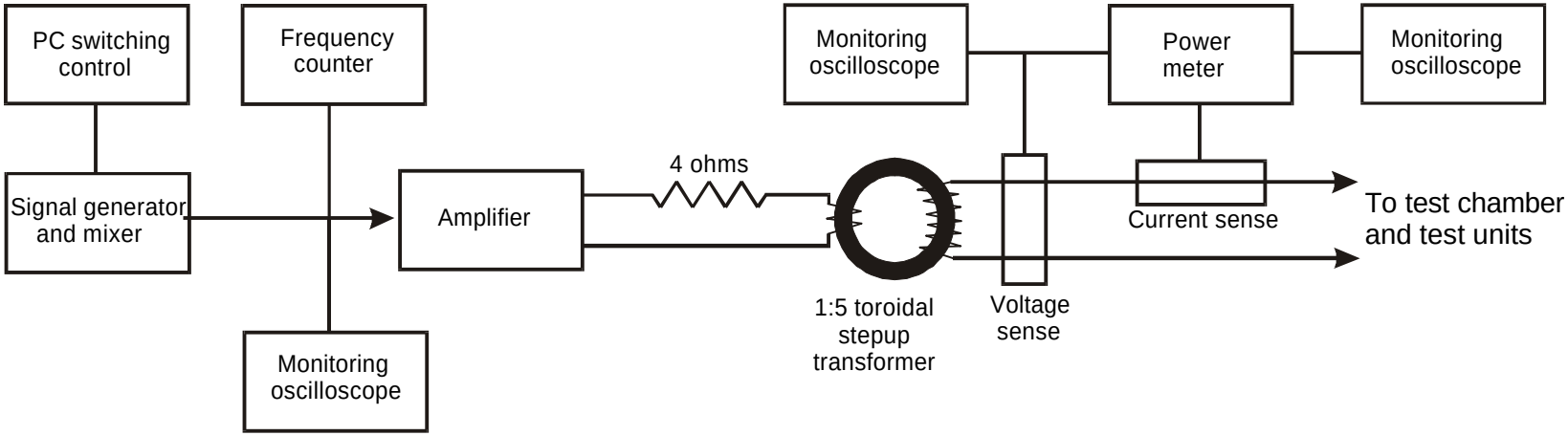

Figure 5. Block diagram of the experimental setup.

Signal generator and mixer

A block diagram of the signal generator and mixer is shown in Figure 6. Although the actual unit contained two additional channels and other capabilities beyond those listed on the diagram, for clarity only those items pertinent to this specific experimental configuration are shown.

An initial sine wave was generated by either an Exar 2206 function generator chip, and passed through a 4 pole Butterworth low pass filter, or was externally supplied. The signal was next split into two channels. In one channel the frequency of the initial signal was doubled via the use of an Analog Devices 633 four quadrant multiplier chip set up as a frequency doubler. A Harris 7216 frequency counter chip and 8-digit display selectively monitored the frequency of either channel. Both the high and low channels contained inverters and phase shifters fabricated from Analog Devices 712 op amps to adjust to any desired phase relationship between the two signals. As the phase shifters tended to alter the amplitude of the signals, their output was routed through automatic gain controls, constructed from Analog Devices 734 and 712 chips, to maintain constant output amplitude. This amplitude could then be altered by a simple variable voltage divider, feeding into an Analog Devices 624 chip for final mixing. Switching of this final output signal was either done manually, or by an external, computer supplied signal.

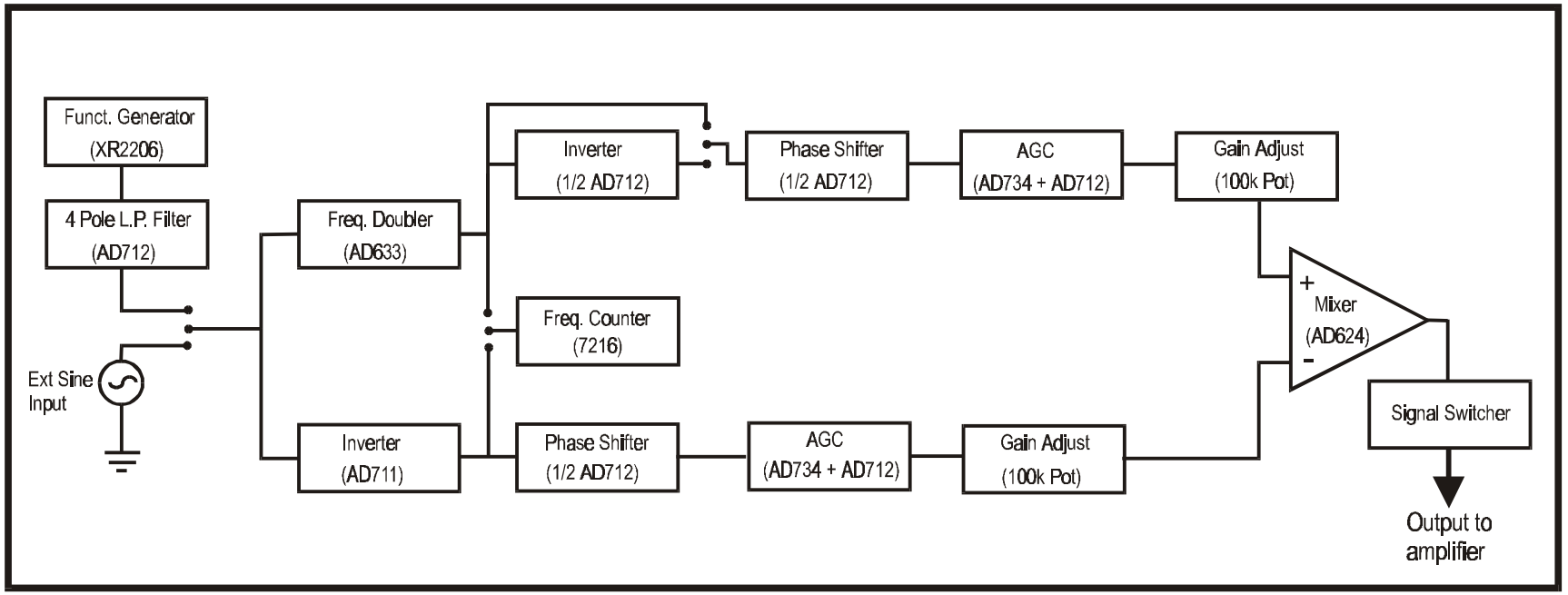

Figure 6. Block diagram of signal generator and mixer.

Test chamber

A cross section of the test chamber is shown in Figure 7 and a close up, annotated photo is shown in Figure 8. The main part of the chamber was fabricated from a 30.5 cm section of 25.4 cm OD clear, cast acrylic tubing. Two 5.71 cm diameter acrylic tubes extended above and below the chamber, enclosing the pendulum fibers. The top and bottom plates of the chamber, as well as the end caps of the upper and lower tubes, were sealed with O-rings and a series of tightening bolts. To minimize the possibility of strong magnetic coupling, all metallic hardware was either brass or stainless steel. Several electrical feed-throughs were provided at various points on the test chamber.

The chamber rested upon a wooden tripod holder with a central hole to accommodate the lower suspension tube. The upper section of the tripod holder was equipped with three leveling screws for chamber position adjustment, resting upon simple vibration isolating material. Initially this material was dense, closed cell foam. But that eventually became overly compressed, and was replaced by discs of “sorbothane” elastomer material approximately 2 cm thick.

Torsion arm suspension

The initial top and bottom torsion fibers were 99.9% pure tungsten, 0.127 mm in diameter and 1.00 meters in length. Tungsten was chosen primarily for its high strength, which allowed its diameter (and thus its torsion constant) to be minimized. The fibers were attached at each end to cylindrical brass plugs 4 mm in diameter and 15 mm long. The fibers passed through holes along the axis of the plugs, and were soldered in place. Due to the small surface area available on the fibers for the solder to adhere to, instances of the upper fiber pulling out of its plugs occurred. This was remedied by passing the fiber completely through the plug, around a small piece of wire, then back into the plug before soldering. The fibers were assembled to their plugs in a jig to ensure identical 1-meter lengths.

The plug at the top end of the upper fiber was clamped with a setscrew into a larger brass holder, which in turn was connected to an electrical pass-through out of the test chamber.

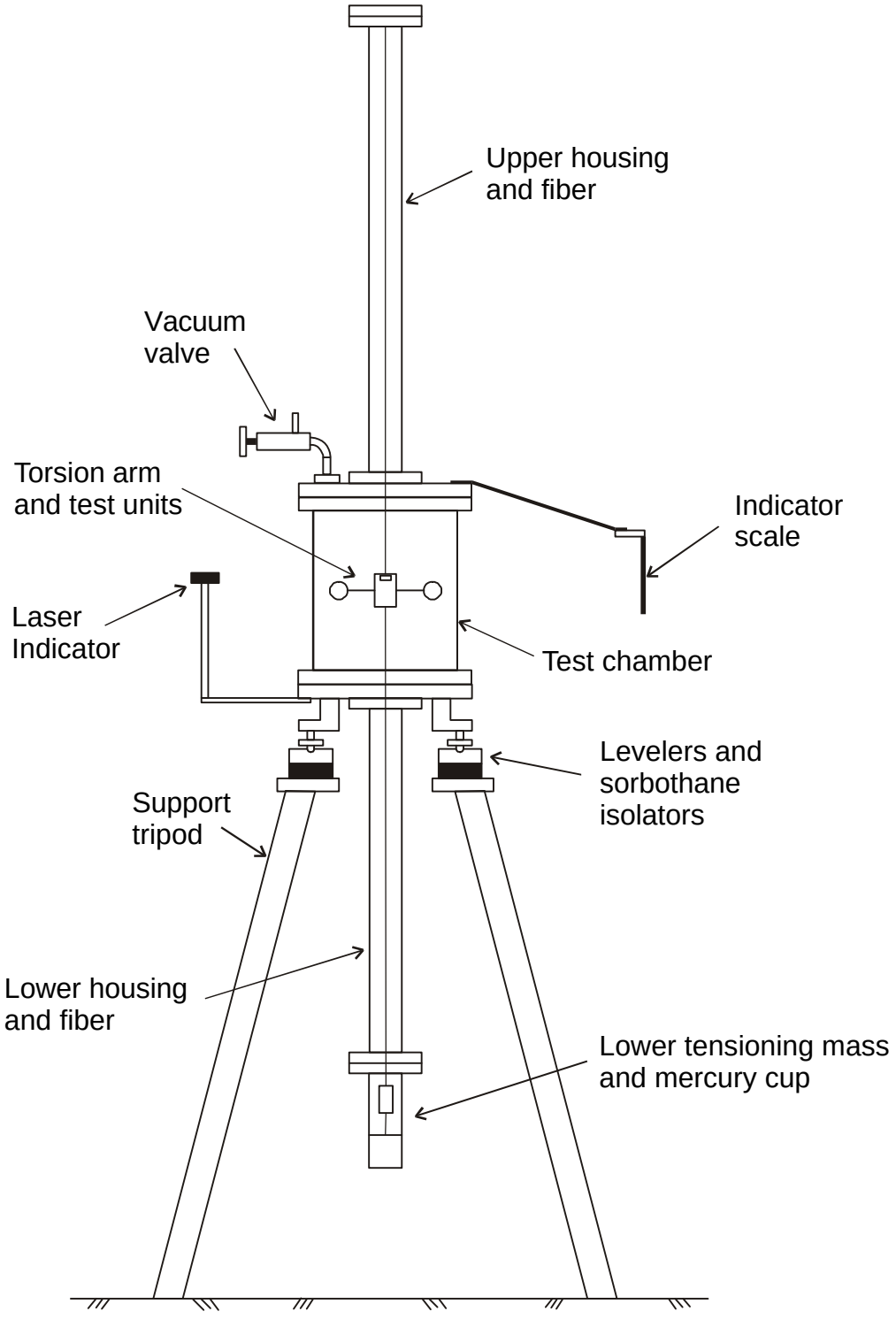

Figure 7. Schematic cross section of test apparatus

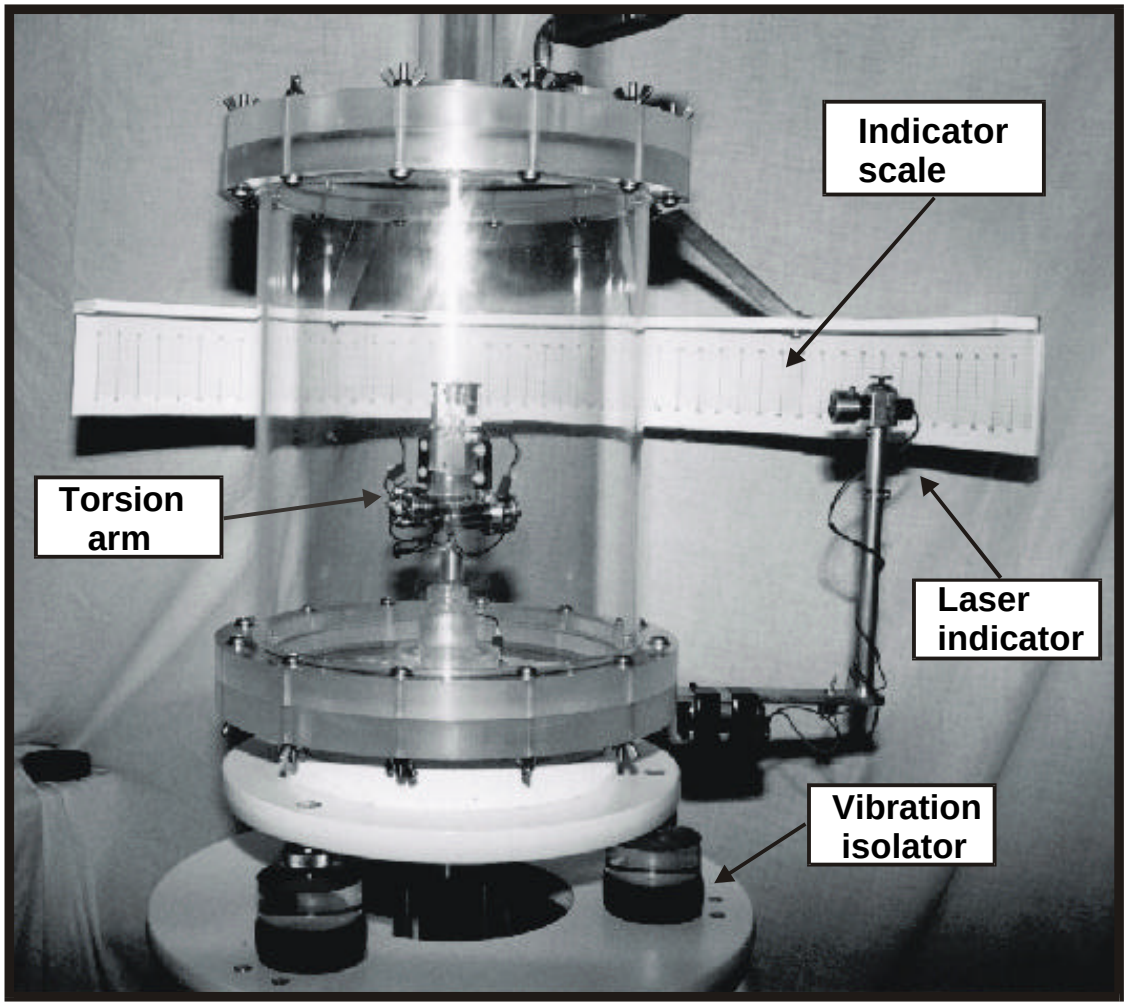

Figure 8. Test chamber.

Initially, the lower fiber was 1 meter in length with the bottom end plug clamped via a setscrew into a cylindrical brass tensioning mass of approximately 84 grams. Beneath that tensioning mass was a configuration that provided an electrical contact into a mercury cup, allowing for limited vertical movement to accommodate thermal expansions or chamber compression under vacuum, and serving to resist rotation of the bottom end of the lower fiber. This lower mechanism proved a source of major problems.

The first design of this contact used a cylindrical mass on vertical rails, the purpose of the rails being the prevention of rotation of the mass and lower fiber. However fabrication imperfections and friction within the rails prevented the mass from moving vertically as smoothly as desired, and spurious movement of the torsion arm resulted. The next design increased the size of the mercury cup, and a device with four vertical vanes, soldered to a central rod beneath the tensioning mass was placed within the mercury. The vanes allowed vertical movement, but to a great extent resisted rotation. Unfortunately, this design revealed that mercury rapidly dissolves solder by literally falling apart after a week. It was replaced by a six-vaned configuration that was precisely machined and mechanically clamped together. Some valid testing was done with this configuration, but it still proved to be less than satisfactory.

Concurrent with refining the lower tensioning arrangement, the suspension fibers themselves required reassessment. The two tungsten fibers had a total series electrical resistance of about 9 ohms. Given operating voltage amplitudes of 200 volts or more, and currents over a half ampere, resistance heating of the fibers in a vacuum turned out to be a substantial problem. During operation, the total 2-meter length of fiber was observed to elongate about 1 cm, indicating an increase in temperature of over 500^{o} C. There seemed to be no obvious lower mechanism that could accommodate this much vertical extension without at least some spurious motion being conveyed to the torsion arm due to mode coupling.

A number of different materials were surveyed as a replacement for the tungsten. The material had to have a low electrical resistivity, yet be strong enough to support the load of the torsion arm and tensioning mass. The least objectionable alternative turned out to be copper. Copper unfortunately has high ductility and isn't as strong as tungsten, but seemed the best compromise due to its very low resistivity. Zirconium-copper alloy holds out promise for future work, as does Copper-beryllium, to a lesser extent.

The minimum size copper wire that could reasonably hold the arm and tensioning mass was found to be 30 gauge (0.25 mm diameter). All else being equal, this reduced the sensitivity to about a fifth of that of the tungsten. Unfortunately, dummy capacitor testing (i.e., the passing of equivalent voltages and currents through the suspension, while the test units are shorted out, as will be discussed in detail later) still showed a small amount of remaining spurious motion. This motion seemed to be some sort of interaction

involving the lower fiber, the vaned arrangement in the mercury and the torsion arm. While its source wasn't obvious, the solution seemed to be to do away with most of the lower fiber altogether. Also the idea of using a multi-vaned contact in the mercury was abandoned.

The final configuration (used in most of the later testing) of the lower fiber was a 5 cm length of 34 gauge (0.16 mm diameter) copper wire, at the end of which was suspended a 32 gm brass tensioning mass. This mass had a very thin brass rod (but no vanes) protruding into a small mercury cup beneath it. The concept was that the lower fiber would provide very little resistance to any torque generated by the arm above. Essentially all torque resistance would come from the upper copper fiber. This had the benefit of increasing the device's sensitivity, although not quite back to the level of the original tungsten arrangement.

Torsion arm

The torsion arm, shown in Figure 9, consisted of a central rectangular portion of acrylic plastic, from which 4 mm OD brass tubes extended. These tubes, as well as the torsion fiber end plugs, were held in place with brass set screws.

Electrical connectivity was provided by tightly twisted wire pairs, passing through the brass tubes to the test units at the ends of the tubes. As the wires entered the center acrylic piece, they were divided so that one wire from each unit was soldered to a brass housing around the lower fiber end plug, and the other two wires soldered to the upper end plug housing. These housings provided electrical connection to the upper and lower fibers.

The points of mechanical connection for the test units were at the outer ends of the brass tubes. These connections were made with nylon and polyethylene spacers that electrically and vibrationally isolated the test units. Later tests included suspending the units from the arms on straps of neoprene material to greatly enhance vibration isolation, over the original vibration isolation mechanisms (which were left in place). Although dimensions varied somewhat during testing, the test units were generally located approximately 7.6 cm radially from the centerline of the test cell for initial tests, and 3.0 cm in later tests. The shorter arm length increased the sensitivity of the device when used in pulsed mode by reducing the moment of inertia of the arm.

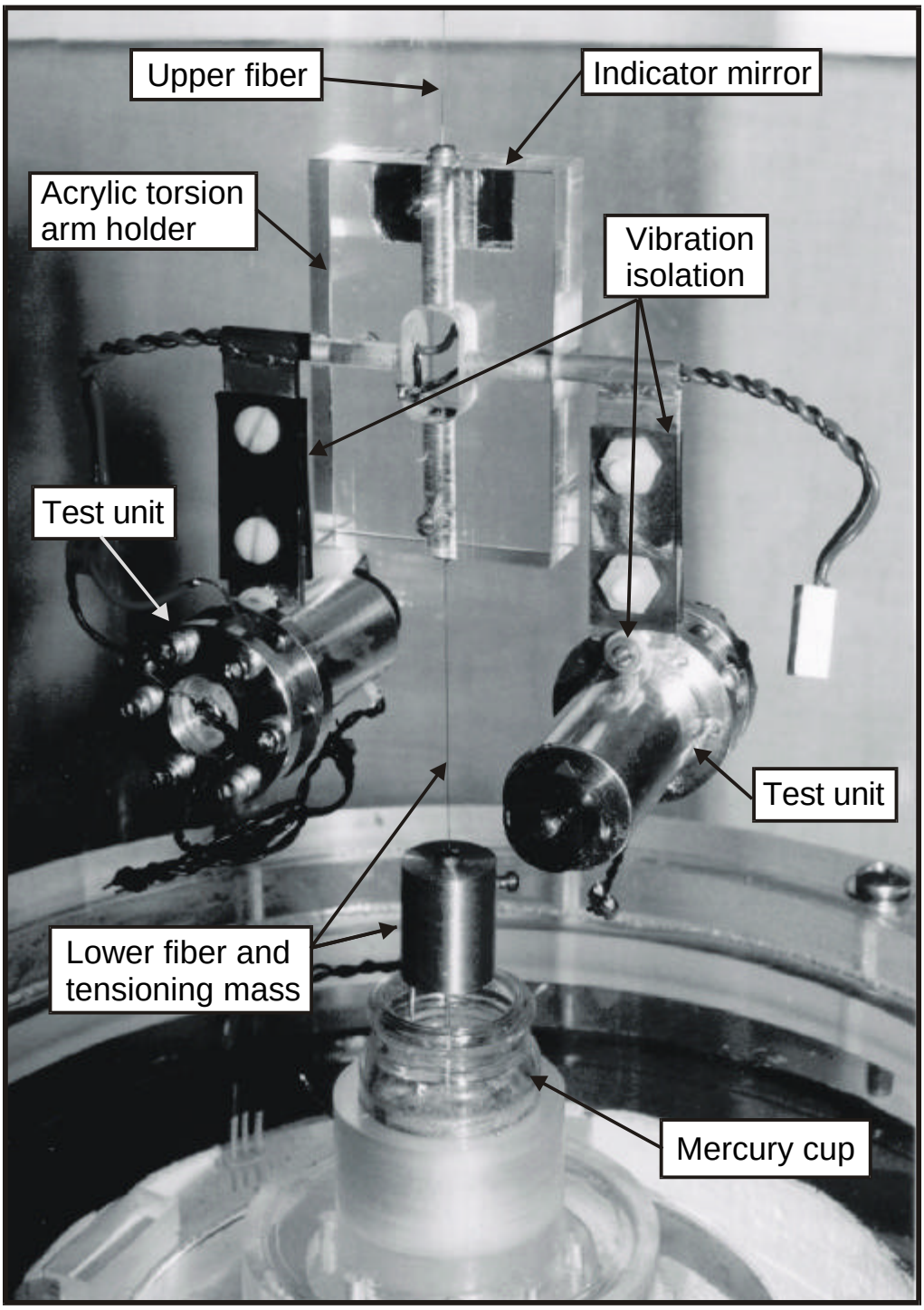

Figure 9. Torsion arm inside test chamber.

Rotation indication

Rotation indication of the torsion arm was performed optically. A laser (a generic red diode laser pointer) was mounted on an adjustable stalk outside the test chamber. The beam was directed into the chamber, reflected off a small front surface mirror above the torsion arm and reflected back out of the chamber onto a circumferentially oriented scale located 45.7 cm from the chamber axis. The scale was scribed in millimeters, and position was resolvable to the nearest 0.5 millimeter. In early data gathering, the position of the indication dot was noted visually and recorded. Later, the scale indications were videotaped, providing a permanent record of each test, and allowing for later, detailed examination of behavior. Also in latter testing, a new scale was placed 137 cm from the chamber axis, increasing the optical lever (and sensitivity) by three times.

Vacuum system

Vacuum was provided by a Duo-Seal model 1400 rotary vane pump capable of achieving a vacuum of 0.1 Torr with the overall system used for this experiment. Vacuum measurements were obtained via a simple mechanical gauge for coarse, high level readings, and a Televac model 2A thermocouple gauge for low level measurements.

Design of test units

Initial design attempts centered around thin, annular PZTs, attached to brass rings, which were envisioned to serve as “resonant amplifiers” for the PZTs. This eventually proved infeasible and abandoned when it was discovered most of the vibratory energy went into circumferential modes rather than the needed longitudinal mode.

The problems of the annular units were overcome through the use of disc PZTs, clamped to a resonant “bar” of appropriate length for a resonant condition. The length had to be long enough to ensure most of the energy went into a longitudinal mode and remained there. The idea was to take the mixed driving signal, apply it to the PZT stack, which in turn drove the resonant bar, which reinforced the vibratory effects occurring in the PZT stack.

The theory predicts the effect should go as the cube of the frequency, so it made sense to design a device that would run at as high a frequency as possible. Given the available electronic resources, a primary frequency of 50 KHz was selected as the “mass-shift frequency”, resulting in a doubled frequency of 100 KHz as the “shuttling frequency”.

The intent was to drive the bar with two superimposed longitudinal waves in a free-free vibratory mode. The bar needed to be of such length such that it resonated at the half-wave length (the fundamental free-free mode) at 50 KHz, and the second harmonic at 100 KHz, (a full wavelength). However not the entire bar would be aluminum. A portion of the bar would consist of clamped PZT discs, with somewhat different acoustic properties than aluminum. This meant it was a hybrid design, and the differing materials had to be appropriately factored.

The final design of the test units is shown in Figure 10. The top diagram is a cross section of a test unit showing the 50 KHz standing longitudinal wave, and arrows indicating the direction of motion. It is apparent that each end of the unit undergoes the maximum displacement, and thus maximum acceleration. It was to be this waveform, operated at a fairly high amplitude, that was hoped would induce a small mass shift in the areas of maximum acceleration. Note that taken by itself, this waveform cancels itself out, and would manifest no resultant force, even if the mass shift effect is real.

The next cross section below in Figure 10 shows the 100 KHz waveform used to provide shuttling action. Note that overall the shuttling action cancels itself out (as well it should), but that the entire stack of PZT discs get moved in one direction at the same time, although to varying magnitude. (It's likely that due to the direct application of a driving electric field to the PZTs, their constituents may be subjected to levels of acceleration above that of the aluminum portions of the bar) Both ends of the unit are moving in the same direction at any point in time, and the center portion is moving in the opposite direction. But examination of the waveform for the 50 KHz signal, the mass-shift signal, shows that there is minimal motion near the center portion of the device, that it is a nodal point. This means the ends are undergoing accelerations of similar magnitude at the same time, and much larger than the center portion. The combination of the 100 KHz shuttling signal moves both ends (presumably undergoing similar mass-shifts) in the same direction at the same time, while moving the center portion (undergoing little, if any, mass-shifts), in the opposite direction. This should result in a net, directional force.

As might be inferred from this discussion, there are many subtleties involved. Unless the candidate device is designed with some thought, a null result is a very likely outcome. This would be the case even if the effect were actually present, as it will simply cancel itself out.

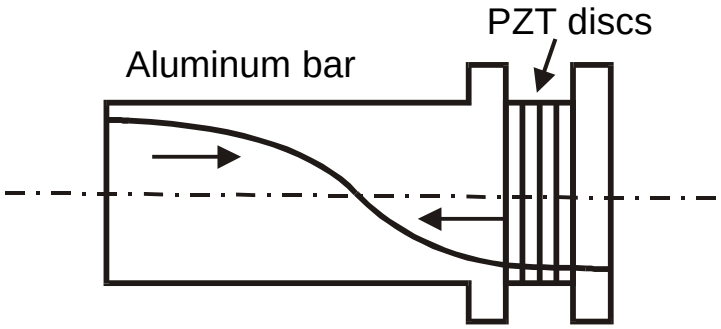

50 Khz mass-shift longitudinal wave

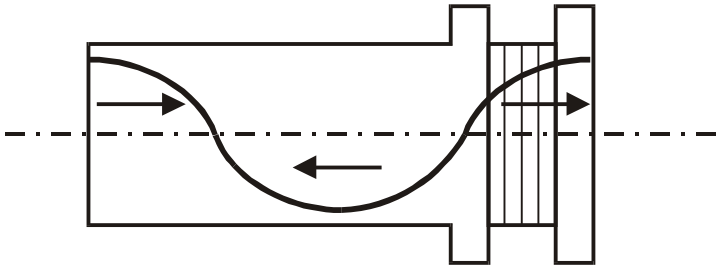

100 Khz shuttling longitudinal wave

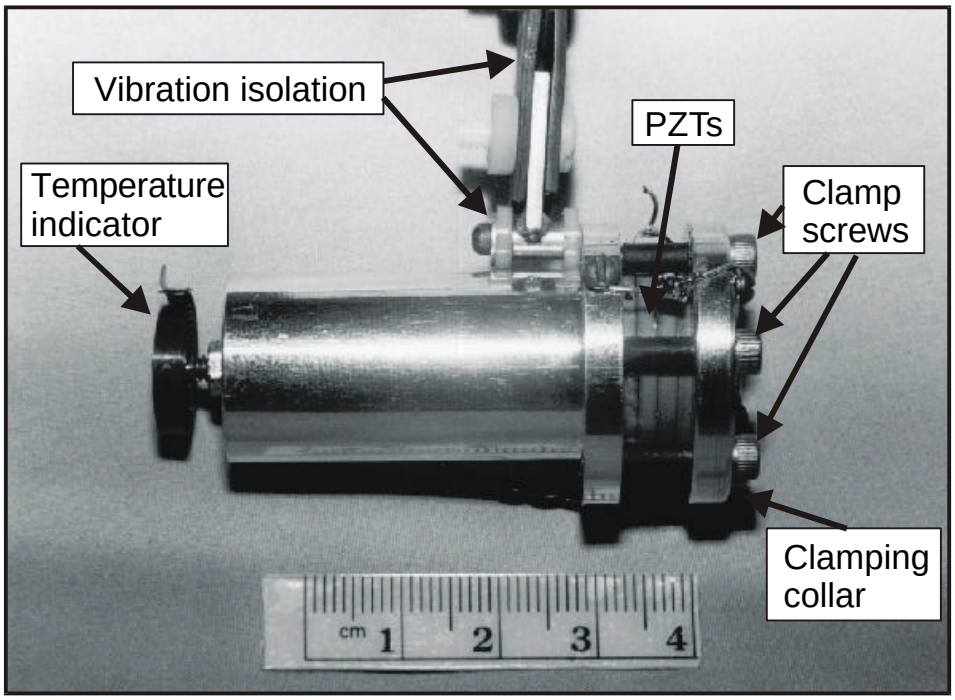

Figure 10. Test unit details. The top two cross sections show the positions of the resonant longitudinal waves within the units at 50 KHz and 100 KHz. The bottom image is a closeup view of a test unit.

In the case of designs such as this, where the resonant bar is comprised of two or more differing materials (aluminum and PZT material), the interfaces can create additional, undesired resonances within the system. For this design, testing showed some longitudinal resonance was occurring within only the aluminum portion of the unit, at a slightly higher frequency than the overall resonance of the unit. Presumably, this was due to reflection at the aluminum/PZT interface. The undesired result of this was the creation of "beating" of the two resonant signals, due to their fairly close proximity. This tends to disrupt the desired resonance.

The design was constrained by the availability of PZT discs, which all had a diameter of 19 mm. This, in effect, set the diameter of the aluminum bar at 19 mm. The material chosen for the bar was 7075 Al alloy. It was selected due to its light weight, acoustic propagation qualities and ease of machining. The final test unit design is shown at the bottom of Figure 10.

The PZT stack consisted of 4 discs (each 1.9 cm diameter x 0.19 cm thick) of axially poled EC-65 lead zirconate titanate material from EDO Ceramics. The discs were separated by thin brass electrodes, and epoxied together using Shell EPON 815C resin and Versamid 140 hardener. This low viscosity epoxy mixture was recommended by the manufacturer of the PZT discs. The stack was clamped to the bar using an annular collar and six 4-40 stainless steel socket head screws. To minimize the possibility of arcing during operation (as the clamping screws were in close proximity to the PZT electrodes), the exposed portions of the screws were covered with heat-shrink insulating material. Eventually, the exposed portions of the PZT stack were painted with high voltage coronal dope to suppress coronal discharge.

The longitudinal acoustic velocity for aluminum is about 5,100 m/sec, and for EC-65 piezo material is about 3,000 m/sec (EDO Ceramics 1998). Given the need for a standing half-wavelength at 50 KHz, and a standing full wavelength at 100 KHz, and a stack of four PZT discs totaling 0.76 cm in length, it was calculated the length of the aluminum "bar" portion should be 3.81 cm in length, and of the same diameter as the PZTs (1.9 cm). While such a relatively short length in relation to the diameter tends to promote other (radial) vibratory modes, the PZT diameter acted as the constraint.

As this design required the passing of longitudinal waves through interfaces of dissimilar materials, acoustical impedances and matching were examined. Aluminum has a bulk acoustical impedance of about 17.3 MRayls[1], and EC-65 PZT material is around 22.2 MRayls. Calculations showed that about 12% of a longitudinal wave approaching an Al/PZT interface would be reflected. While this is higher than desired, the lack of

[1] A Rayl is a standard measure of acoustic impedance with the units of kg/m^2sec. The characteristic acoustic impedance of a material is equal to its density multiplied by the sound velocity within the material.

readily available alternative materials, providing a better match, forced the acceptance of this situation.

Operating temperature of the units was a major concern. EC-65 material has a Curie point of 350º C. This is the temperature at which the material becomes de-poled and permanently loses its piezoelectric properties. As significant power levels were anticipated, as well as operation in a vacuum, it was apparent the temperature of the units needed to be monitored to avoid de-poling the PZTs. This was accomplished by the addition to the end of the test units of a simple spiral, bimetallic strip temperature indicator, liberated from a kitchen thermometer. By calibration in an oven, it was possible to determine the position of the indicator that signified the maximum temperature limit had been reached.

Accelerometers

In order to check for resonance conditions within the test units, small piezoelectric accelerometers were developed. These units, shown in Figure 11, were about 3 mm square and fabricated from essentially scrap chips of EC-65 PZT material less than 1 mm thick. To construct an accelerometer, two of these PZT chips were assembled with epoxy into a "sandwich", with a thin brass electrode in between. A slightly thicker, grounded piece of brass was epoxied on top, serving as both a driving mass and an electrode. This driving mass provided force on the PZT chips as it accelerated during operation. Leads had to be soldered to the electrodes prior to assembly, to avoid de-poling the PZT material from the heat of the soldering iron. The unit was then glued to a surface under study with cyanoacrylate adhesive. In some cases, each accelerometer was covered with a thin, grounded brass shield to prevent RF pickup, and the output run via thin, shielded cables to oscilloscopes for monitoring. In most cases, however, this additional shielding was found to be unnecessary. These simple devices worked exceedingly well, producing signals with peak amplitudes in the 1 volt range when running at 100 kHz and could be monitored without preamplification by simple oscilloscopes. Because the leads from the accelerometers would have interfered with operation of the torsion arm, accelerometers mounted on the test units were only used for resonance monitoring when the test units were in static test stands.

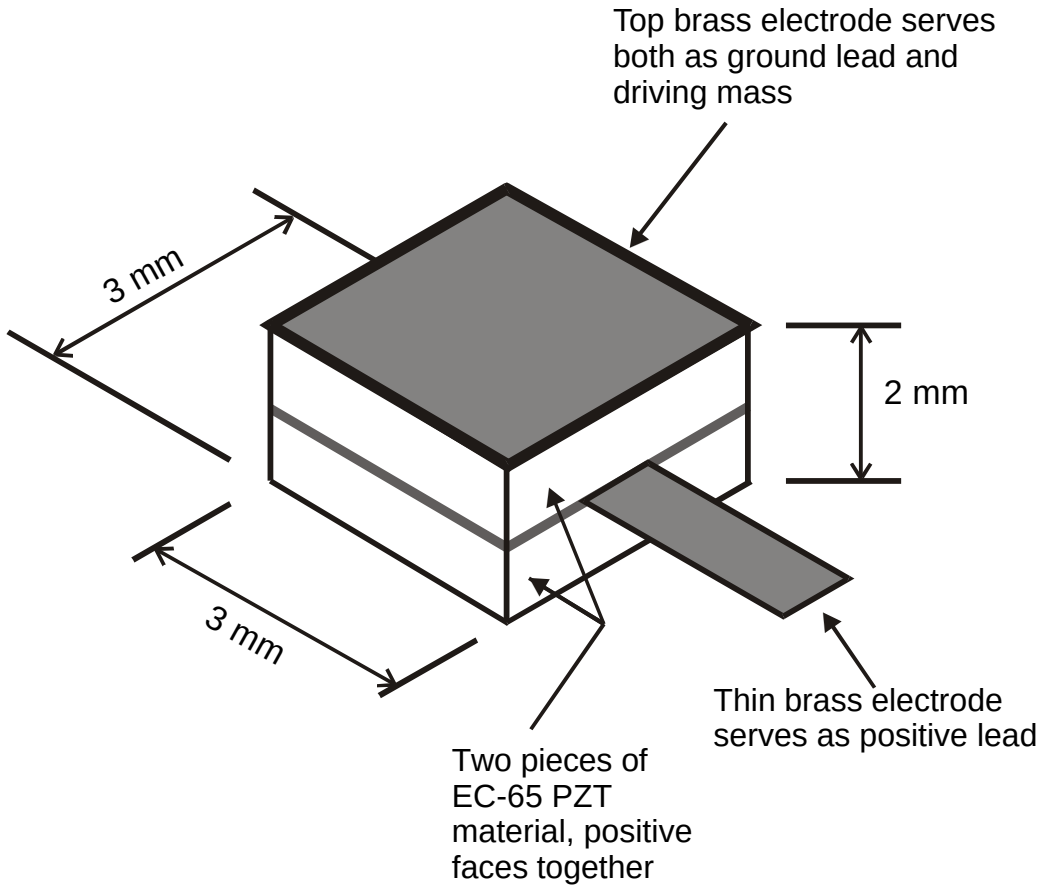

Figure 11. Accelerometer detail. The accelerometer is attached to a grounded surface. Omitted for clarity is a ground lead from the top electrode to the surface the unit is attached to.

IV. Methodology

Data gathering was fairly uniform and consistent. The torsion arm was allowed to come to as complete a stop as possible prior to beginning any test. Usually this required quite some time as the damping rate was quite low, and occasional building shake contributed to the motion. The process could be speeded up a bit by placing a strong magnet just outside the test chamber for very brief, strategically timed intervals. The magnet was strong enough to weakly attract the stainless steel hardware, and after some magnet-waving experience was developed, it was possible to bring the arm almost to rest using this method alone.

Prior to testing, the final mixed output of the two signals (one at twice the frequency of the other) was adjusted to result in a sort of poor looking sawtooth wave. Ideally, the signal applied to the PZTs should closely match the signal coming out of the signal generator. Unfortunately, equipment limitations greatly altered the signal by the time it was fully amplified. Part of the signal distortion was caused by the amplifier's tendency to attenuate the high frequency component much more than the low frequency component. The other source of signal degradation was the need to pass the output of the amplifier through a toroidal step-up transformer. This tended to round off rapid changes in the signal, precisely the sort of sharp signals that could be theoretically expected to induce mass shifts. Ultimately, a sawtooth wave, due to its asymmetry, provided the best available substitute.

Most of the later, formal testing was recorded on 8mm videotape to maintain a record, which also allowed for more detailed examination of the results. The laser indicator was usually recorded for about 2 minutes prior to any energization, to provide a baseline condition.

The test units were usually energized in a series of three five-second pulses. The reason for not applying any longer pulses was the need to maintain reasonable operating temperatures in the test units. 15 seconds of energization (the result of one test sequence) usually required at least 30 to 45 minutes to cool in the vacuum chamber. The length of the pulses was computer controlled to maintain a constant 5 seconds (or whatever value was selected) throughout the test.

Application of the pulses during early testing was done manually. As the first pulse was applied, initial motion was usually apparent and a specific direction of the apparent force discerned. The triggering of the second and third pulses was timed so the torsion arm was just beginning its swing in the same direction caused by the first pulse. Like giving a child on a swing repeated pushes, this had the effect of magnifying the effects of

individual pulses. Later testing was given over wholly to computer control, which resulted in an unexpected validation, to be discussed later.

As the pulses were applied, the motion of the laser indicator dot was recorded on videotape. After completion of the entire pulse sequence, the motion of the laser indicator was recorded for several minutes further to acquire an "after" baseline. Utilizing this basic technique, a number of different configurations were tested. These included different length torsion arms, and two different test unit designs. However before formal testing could be begun, the torsion arm required calibration.

Calibration of torsion arm

A torsion pendulum may be used in two different modes: static or dynamic (or ballistic). In the static mode, the pendulum is initially at rest, and an external force is brought to bear against it. The pendulum will then deflect until the torsion provided by the fiber balances the torque created by the external force and equilibrium is reached. In the dynamic mode, the pendulum is given an external torque during part of the swing, altering the amplitude of any existing oscillation.

To calibrate for either mode, it was first necessary to find the suspension fiber's torsional stiffness. To do so, the oscillation period of a calibration arm of known moment of inertia had to be measured. A calibration arm, as shown in Figure 12, was constructed, and its total moment of inertia was calculated from the individual components. The value for its moment of inertia was found to be 7.35×10^{-4} kg-m^2. Its period of oscillation in a vacuum, averaged over 6 cycles, was found to be 33.4 seconds.

It was assumed this configuration, operating in a vacuum, acted essentially as an undamped torsion pendulum. Observations of its long-term oscillatory behavior confirmed this. Very little damping occurred.

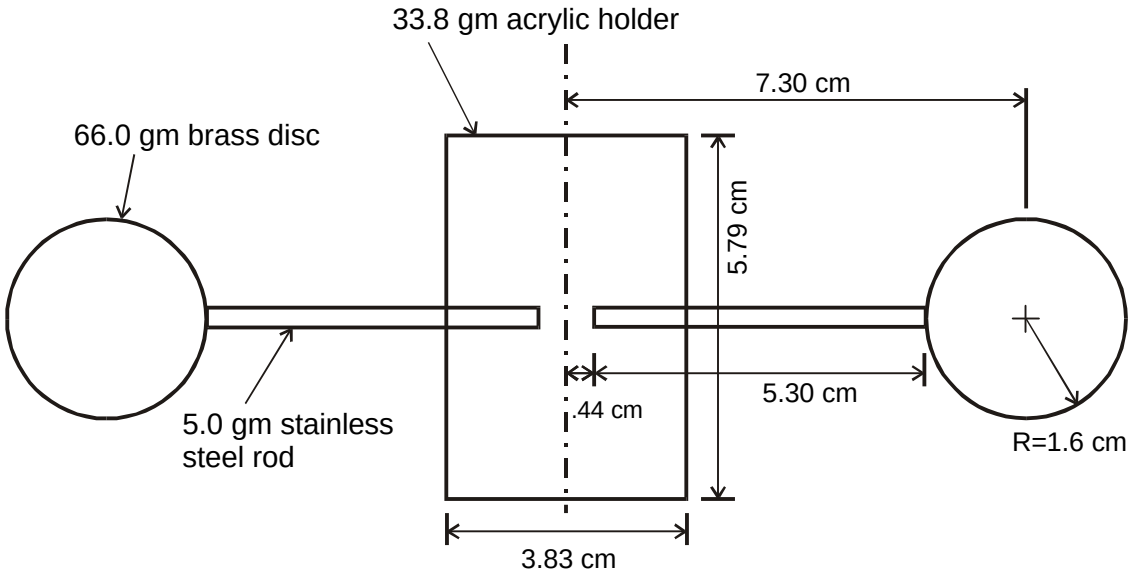

Moment of inertia of acrylic holder = 1.36×10^{-6} kg-m^2

Moment of inertia of rod = 4.78×10^{-6} kg-m^2

Moment of inertia of brass disc = 3.56×10^{-4} kg-m^2

Total moment of inertia = $I_{Holder} + 2 \times (I_{rod} + I_{Disc})$

Total moment of inertia = 7.35×10^{-4} kg-m^2

Oscillation period (Average of 6) = 33.4 seconds

Figure 12: Torsion fiber calibrator. The moment of inertia of this calibration arm as computed above, combined with its period, allow for the calculation of the fiber's stiffness, and thus calibration of the entire apparatus.

For a torsion pendulum, the torsional stiffness, S, is given by (Talley 1991):

$$S = \frac{Q}{q} = I\frac{4p^2}{T^2} \tag{4}$$

where

Q = Total torque in N-m;
q = Angle of twist of calibration arm and fiber in radians;
I = Moment of inertia of the suspended mass in kg-m^2;
T = Oscillation period in seconds.

As a result, S for the 1 meter copper fiber utilized, was calculated to be 2.6 x 10^{-5} N-m.

To find the amount of force necessary to deflect the indicator dot a specific amount on the scale in the static mode of operation, it is necessary to combine three expressions:

$$q = \frac{\Delta x}{2r} \tag{5}$$

$$Q = Sq \tag{6}$$

$$F = \frac{Q}{nR} \tag{7}$$

where

Δx = Change in scale indication from rest to deflected in m;
r = Mirror to scale distance (0.457 m);
q = Angular twist of arm and fiber in radians;
S = Torsion stiffness of fiber in N-m;
Q = Total torque on fiber in N-m;
R = Moment arm of test units about fiber axis in m;
n = Number of test units energized on arm (1 or 2, but normally 1);
F = Force produced by each device in N.

Combining these expressions gives:

$$F = \frac{S\Delta x}{2nrR} \tag{8}$$

Thus the amount of force required to produce a given static mode scale deflection may be determined.

With one test unit operating at an arm length of 75 mm, a 0.5 mm deflection (the resolution limit) of the scale indicator would be produced by a force of 1.9×10^{-7} N or 0.019 dynes (0.02 milligram-force). This would be the minimum force resolvable in the static mode, assuming the test unit was energized long enough to allow the deflection of the arm to reach equilibrium.

While this gives some indication of the resolution of the test apparatus, the actual behavior is not quite so simple. The previous analysis assumes the displacement reaches an equilibrium position. However, given the extremely low damping, and the necessarily short periods of energization, a briefly acting force will simply send the torsion arm into a series of oscillations. This is, in essence, an undamped, harmonic oscillator driven by a non-periodic step force function. Analysis of this behavior, though a bit more complex, results in a much more accurate model of the behavior.

Harker (1983) provides a good derivation and discussion of this type of oscillation. Specifically, he shows that an undamped linear harmonic oscillator initially at rest, subjected to a constant force of finite duration, will reach a maximum displacement of:

$$x_{max} = 2\left(\frac{F}{K}\right) sin\left(\frac{w_1 T_{Pulse}}{2}\right) \tag{9}$$

Where:

x_{max} = Maximum displacement from rest position.
F = Force of constant amplitude applied to oscillator.
K = Spring constant of oscillator.
w_1 = Natural frequency of oscillator.
T_{Pulse} = Length of time the force is applied.

Through the use of angular-linear analogs, this equation may be easily converted for use with torsional oscillators by appropriate substitutions.

$$q_{max} = 2\left(\frac{Q}{S}\right) sin\left(\frac{w_1 T_{Pulse}}{2}\right) \tag{10}$$

With q_{max} being the maximum angular displacement from rest, and all other variables as previously defined.

To further convert Eq. 10 to a directly useful form, a few other substitutions may be made.

$$q_{\max} = \frac{\Delta x_{indicated}}{4\mathrm{r}} \tag{11}$$

$$\mathrm{Q} = \mathrm{F}_{\mathrm{unit}}\ \mathrm{R}\ \mathrm{n} \tag{12}$$

$$w_1 = \sqrt{\frac{\mathrm{S}}{\mathrm{I}}} = \frac{2p}{\mathrm{T}} \tag{13}$$

Where:

$\Delta x_{indicated}$	=	Observed excursion of laser indicator dot on scale (peak to peak) in meters.
r	=	Mirror to indicator scale distance in meters.
$\mathrm{F}_{\mathrm{unit}}$	=	Force generated by single test unit in newtons.
R	=	Moment arm of test units about fiber axis in meters.
n	=	Number of test units energized on arm (1 or 2, but normally 1).
S	=	Torsion stiffness of fiber (2.6×10^{-5} N-m).
I	=	Moment of inertia of test devices and torsion arm in kg-m^2.
T	=	Oscillation period in seconds.

Substituting Eqs. 11, 12 and 13 back into Eq. 10, and rearranging, results in:

$$\mathrm{F}_{\mathrm{unit}} = \frac{\mathrm{S}\,\Delta x_{indicated}}{8\,\mathrm{r}\,\mathrm{R}\,\mathrm{n}\,\sin\left(p\,\frac{\mathrm{T}_{\mathrm{Pulse}}}{\mathrm{T}}\right)} \tag{14}$$

The argument of the sine value is in radians and $\mathrm{T}_{\mathrm{Pulse}} \le \mathrm{T}$.

This allows for calculation of the amount of force produced on the basis of a single pulse, with the torsion arm initially at rest. However in most cases, multiple pulses were applied to the test unit(s). This is a much more difficult problem to deal with, as the initial conditions (i.e., position and velocity of the torsion arm) for subsequent pulses are not well known.

To deal with this, at least to an approximation, it was decided to measure the total energy contained within the oscillating system, after all the pulses were applied, on the basis of the amplitude of the final (usually, but not always the peak) oscillation. Then the

total energy was divided by the number of applied pulses to obtain an average "energy per pulse" added to the system. Finally, on the basis of this average imparted energy, an equivalent, single oscillation amplitude for one pulse could be calculated. This oscillation amplitude was then inserted into Eq. 14 for computation of a force value.

The total energy, E, in an oscillating system as a function of the amplitude of oscillation, A, is given as:

$$E = \frac{1}{2} K A^2 \tag{15}$$

Dividing the total amount of energy by the number of pulses, P, and solving for A, gives the equivalent amplitude, A_{equiv} , of one pulse:

$$A_{equiv} = \frac{A}{\sqrt{P}} \tag{16}$$

Keeping in mind that $A = \Delta x_{indicated}$ an equivalent Δx for one pulse may be obtained dividing $\Delta x_{indicated}$ by $\sqrt{P}$. This may be substituted into Eq. 14 to determine the approximate force produced by a test unit during P pulses, and is the basis of all force calculations done during testing:

$$F_{unit} = \frac{S \Delta x_{indicated}}{8 r R n \sqrt{P}\, sin\left(p \frac{T_{Pulse}}{T} \right)} \tag{17}$$

Validation protocols

Preliminary testing showed immediate, obvious motion of the torsion arm. However that is not necessarily an indication of a thrust-like force, as there are other possible causative agents of the observed motion. Fortunately, because torsion pendulums are essentially very simple devices, there are only a limited number of possible sources of spurious motion. It was possible to devise a set of simple tests to exclude mundane causes of arm rotation.

Possible sources of spurious motion include:

- Sonic wind

- Image charges
- Coupling to external electromagnetic fields
- Coronal discharge
- Electrostrictive effects
- Thermal effects on suspension
- Mechanical resonance couplings

A sonic wind (also known as acoustic streaming) is a phenomenon occurring in gaseous or fluid mediums subjected to high intensity sound waves (Frederick 1965). As the sound wave propagates from the source, the regions of compression end up having a greater velocity than the rest of the wave, and an asymmetrical sawtooth wave results. This is exacerbated when the driving signal itself has a sawtooth form. The effect can create a "D.C." flow of the medium, sometimes of significant velocity. Earlier experiments had clearly shown this to be occurring with some test units at normal atmospheric pressure, which led to the decision to do all testing in a soft vacuum.

To check for the presence of sonic wind, the test units were operated at several different vacuum levels, ranging from 0.2 Torr to 74 Torr. Above 2 to 5 Torr, effects of a sonic wind nature were observed, and tended to increase as the pressure increased. Below 2 Torr, no effects were observed. As all normal testing occurred at vacuum levels between 0.12 Torr to 0.3 Torr, it may be concluded that sonic wind was not a factor.

An image charge is an induced electric surface charge set up in an adjacent conductor, due to the presence of a body with an initial electric charge. Image charges are opposite in polarity to the initial charge, and thus act to attract the body possessing the initial charge. While the operating voltages of the test devices were not very high (typical amplitudes less than 250 volts), there were steel cabinets a few meters away, as well as other conductors, so this was considered as a possible source of motion.

To determine if image charges were playing any part in the observed motion, a thin 30 cm by 50 cm aluminum plate was placed immediately adjacent to the outer wall of the test chamber, 10 cm to 20 cm from the torsion arm, as the test units were energized. This was done with the plate in several different orientations relative to the arm, including above it. In none of the tests did the arm manifest any apparent reaction to the close proximity of the aluminum plate. If such a close conductor had no effect on the arm's motion, it could be concluded that other, more distant conductors would also have no effect, and thus could be ruled out as a source of observed motion.

Coupling to external magnetic fields (specifically that of the Earth) was a minor, but investigated, concern. Since the signal driving the test units was alternating, any generated magnetic field would be expected to cancel itself out. But since the signal was very non-uniform, a test was devised to examine this possibility. A large magnet was placed level with the torsion arm, 35 cm from the center axis of the test chamber. This was the distance at which the magnet was found to deflect a magnetic compass 90 degrees, clearly overpowering the Earth's ambient magnetic field. The test units were energized with the magnet in line with the torsion arm and again with the magnet at right angles to the arm. Neither configuration caused any sort of behavior of the arm different from when the magnet was not present. This conclusively rules out any possibility of motion being caused by interaction with the Earth's magnetic field.

Presence of coronal discharge was checked for by applying a sinusoidal signal to a test unit, then slowly increasing the signal amplitude while observing the unit in darkness. For a given vacuum level, a purple-violet glow discharge began at fairly well defined voltage levels, quickly followed by arcing discharge. The table immediately below shows the peak-to-peak voltage levels at which coronal discharge just became visually perceptible. The available equipment limited the maximum test voltage to around 700 volts peak to peak.

Vacuum (Torr)	20	10	1.0	0.40	0.30	0.20	< 0.20
Breakdown Voltage (p-p)	> 700	480	480	500	550	700	700

During normal testing, most vacuum levels ranged from 0.12 Torr to 0.3 Torr, and maximum applied peak-to-peak voltages were 525 volts or less. As this was approaching the measured breakdown limit, high voltage coronal dope was applied to all exposed conductors exposed to high voltage levels. With this additional level of insulation, no discharges of any sort were observed during formal testing. Thus any sort of reaction effect due to coronal discharge may be excluded as a possible source of torsion arm motion.

It should be noted that coronal discharge is not the same as "ion wind". Ion wind is the acceleration of ionized residual air molecules by very high voltage static potentials. Given a high enough static potential, significant forces may be generated by such an effect. However given the relatively modest voltage levels utilized in testing, and the fact the voltage potentials were oscillatory, not static, ion wind was not a possible source of motion in this apparatus.

Suspension effects, which encompass thermal and electrostrictive effects, were a significant problem with this apparatus. The great bulk of the initially observed motion proved to be thermal, not electrostrictive, as might be expected. Electrostriction is a phenomenon occurring in almost all materials to varying extents. It is an elongation of a

material proportional to the square of the applied voltage. Unlike the piezoelectric effect, which is linear, electrostriction is a quadratic effect. Fortunately, electrostriction is usually a very small effect, even in materials where it is at its greatest, such as those of crystalline structure. In the fairly ductile copper wires used for this suspension, electrostriction is essentially negligible and may be dismissed as a suspension-induced effect.

To test for suspension-induced effects, a very powerful protocol was developed using “dummy capacitors” located external to the test chamber, but still in series with the electrical circuit. Capacitors with a value of 0.01 uF were selected to closely duplicate the voltages and currents measured in the circuit supplying the test units during the unit’s operation. The test units were then shorted out, and the capacitors added in series to the circuit, external to the test chamber. Thus the same voltages and currents were flowing through the suspension wires, and through the arms to the test units, but the test units weren’t actually energized.

This protocol revealed a number of shortcomings with early suspension designs resulting in spurious motion (as already discussed), but led to a final, reliable design. Most preliminary tests were performed at power levels around 75 watts. Dummy capacitor testing with 100 KHz signals showed the suspension supported this power level with no motion. The power level was then increased to 140 watts, almost double that of normal testing, and still no motion of the torsion arm resulted. It may then be reliably concluded that the suspension does not impart any sort of rotation to the torsion arm, at least up to power levels of 140 watts, well above the level of any of the formal testing. Thus suspension thermal expansion, thermal rotation, electrostriction, and any other suspension-specific effect, caused by the presence of voltage or current, may be excluded as a source of motion

Finally, mechanical resonance couplings were considered. It’s not immediately obvious how a high frequency vibration at the ends of the torsion arm could couple to the mercury cup or the upper suspension, resulting in rotation. Still, it was considered possible there could be some strange coupling going on, resulting in rotational motion. This was dealt with initially by connecting the test units to the arms with simple polyethylene sleeves and nylon washers to attenuate transmission of high frequency vibrations. Later that was enhanced by also suspending the units from thin strips of neoprene. Finally, testing showed (see for example Table 1, Test number 7) that when the units were turned from a horizontal to a vertical orientation on the arms, rotational motion ceased. Yet the units were still vibrating. If the motion were some sort of mechanical vibratory coupling, the motion should have remained. Thus mechanical vibration couplings between the test units and the suspension/chamber, may be excluded as a possible source of motion.

In summary then, through either testing or re-engineering, motion due to sonic wind, electromagnetic couplings, suspension effects and vibrations all could be reliably dismissed as sources of motion. Yet significant amounts of motion could still be observed when the test units were energized. This strongly suggested either a real effect was occurring, or there was some other mundane source of motion that had been overlooked, and managed to slip through the validation protocols.

V. Results and Analysis

Initially the plan was to operate both units on the torsion arm at the same time, the idea being that both would contribute equally toward rotation of the arm, and any effect present would be much more pronounced. However preliminary testing showed rather erratic behavior. In some cases, significant rotation in one direction was noted, and later, the observed rotation had reversed. Despite great care to construct the test units as alike as possible, it was suspected the two units had operating characteristics different enough to result in situations where one could partially or wholly cancel the other out, if an effect was being generated. Because of this, it was decided to operate the test units one at a time, the other unit not being connected and merely present to provide a counterbalance on the arm.

The data from the testing sequences is displayed in the following tables. The tests are numbered in the sequence they occurred, although in some cases considerable time elapsed between them. The tables don't show the great deal of data used for validation testing and refinement of the suspension. Only after the test apparatus was reliably rid of spurious motion did formal data gathering commence. In some cases, as an oversight, the vacuum level was not recorded. Those cases are denoted in the tables as "NR". Typically, the vacuum level would have been in the 0.2 to 0.3 Torr level for those tests. Finally, all force calculations were made using Eq. 17. In the few cases where later pulses in the testing sequence reduced an oscillation, the mid-test, highest amplitude was used in the force calculations, along with the number of pulses that created it. This situation occurred in the supplemental testing.

Tests 1 through 7, shown in Table 1, show the results for the first seven formal testing sequences. The first 5 tests show a consistent counterclockwise (CCW)[2] rotation. The first two tests are essentially duplicates of each other, all parameters being held constant as closely as possible, except for the phase relationship of the high and low frequency signals. For Test 2, that phase relationship was reversed from Test 1. Theoretically, this should result in a force reversal, yet this was not observed, although the oscillation amplitude diminished by a third. Test 3 returned the phase relationship back to that of Test 1, and the oscillation amplitude increased almost back to that of the recorded Test 1 level. While this is somewhat suggestive of a phase reversal, it falls far short of what would be expected.

Test 4 consisted of the application of a pure sine wave at the mass-shift frequency only. Interestingly, this resulted in rotation that was a significant percentage of that

[2] See Figure 9 for torsion arm configuration corresponding to CW or CCW rotation.

observed with a mixed signal. This isn't entirely unexpected. Since the test units were designed to resonate at both 50 KHz and 100 KHz, strong excitation with a 50 KHz signal (the mass-shift frequency) would likely also stimulate vibrations at the 100 KHz frequency, somewhat duplicating the effects of a mixed signal, although with no control over the phase relationship of the two signals. Test 5 examined the sensitivity to changes in frequency and found it was not terribly sensitive.

Test 6 looked for response changes due to long term settling of the test units. It often occurred that when first energized, after sitting for a lengthy period of time, the test units exhibited anomalous behavior or zero offsets. A zero offset is when an oscillation occurs, but is not centered on the initial starting point, and eventually comes to rest at some point other than where it began. This only occurred, those times it did happen, when the test unit had sat undisturbed in the test chamber for long periods of time, or the entire apparatus had just been reassembled. After an initial display of a zero offset, it would go away. While Test 6 did not show an offset, it did display evidence of long-term "drift" effects within the test units. That is, the direction of the rotation reversed, although weakly.

The final test with the initial vibration isolation was Test 7. In this test the units were rotated on the arm from their horizontal orientation to the vertical. When energized, no rotation was detected. This test suggests that whatever is producing the apparent force on the arm, is in the horizontal plane of the test units, and is not some sort of mechanical resonance coupling with the suspension.

The next sequence of testing, Tests 8 through 17, are summarized in Table 2. These tests added additional vibration isolation by hanging the test units, with their original vibration isolation still in place, from short strips of neoprene.

Tests 8 and 9 continued to show the CCW rotation observed in most of the prior tests. As a check of long-term drift changes, the apparatus was allowed to set undisturbed for 12 hours, and then Test 12 was performed. It continued to show a CCW rotation, but was noticeably diminished.

As an attempt to create consistent thermal conditions within the test unit from test to test, thus reducing drift, a simple cooling protocol was tried. After Test 10, the chamber was flushed with air for 10 minutes, then underwent a 15-minute pump down, after which the next test was immediately begun. It was hoped this repetitive procedure would result in similar thermal conditions within the PZT stack from test to test. The 15-minute pump down tended to leave the vacuum level a little higher than desired, but still well below that at which any sonic wind effects should occur.

Test #	Frequency (KHz)	Power (Watts)	Vacuum (microns)	Final oscillation amplitude (mm)	Force (dynes)	Notes
1	51/102	84	140	3.5 CCW	0.038	
2	51/102	77	130	2.0 CCW	0.022	Same as Test 1, but phase relationship of signals reversed.
3	51/102	82	140	3.0 CCW	0.032	Same as Test 1.
4	51 only	84	130	2.0 CCW	0.022	Pure 51 KHz sine wave only.
5	53/106	78	130	2.0 CCW	0.022	Check of frequency sensitivity.
6	51/102	87	140	0.75 CW	0.008	4 - 5 second pulses, sat for 36 hours prior to test.
7	51/102	87	NR	0	0	Test units rotated to vertical orientation on arm. No motion detected.

Table 1. Experimental data using initial vibration isolation. Power application consisted of three pulses of five-second duration unless otherwise noted. All tests began with initial oscillation less than 0.5 mm. Oscillation period = 30 seconds, r = 0.457 meters, R = 0.075 meters.

Test #	Frequency (KHz)	Power (Watts)	Vacuum (microns)	Final oscillation amplitude (mm)	Force (dynes)	Notes
8	51/102	89	NR	0.5 CCW	0.0048	
9	51/102	89	NR	1.0 CCW	0.009	
10	51/102	91	NR	0.5 CCW	0.0048	Unit sat for 12 hours prior to test.
11	51/102	91	330	2.5 CW	0.024	Flushed with air for 10 minutes, then 15 minute pump down.
12	51/102	91	340	0.5 CW	0.0048	Repeat of Test 11.
13	51/102	90	300	0.5 CW	0.0048	Repeat of Test 11.
14	51/102	89	180	< 0.5 CW	0	No air flush, remained in vacuum for 30 minutes prior.
15	51/102	90	160	0.75 CCW	0.007	No air flush, remained in vacuum for 37 minutes prior.
16	51/102	89	250	< 0.5	0	Repeat of Test 11. Direction of motion indiscernible.
17	51/102	87	250	1.5 CW	0.013	Repeat of Test 11.

Table 2. Experimental data after addition of enhanced vibration isolation to test units. Tests 10 through 17 were conducted in close sequence. Power application consisted of three pulses of five-second duration. All tests had initial oscillations less than 0.5 mm. Oscillation period = 26 seconds, r = 0.457 meters, R = 0.075 meters.

Test 11 showed a reasonably large oscillation of 2.5 mm, but now in a CW direction. A possibility considered for this large excursion was the trapping of air in the silicone grease beneath the retaining collar of the PZT stack, during the flushing phase of cooling. It was thought perhaps the vibrations generated by the PZT stack could then release the trapped air, resulting in a small reaction, like a spacecraft thruster. This didn't seem to be a possibility in this case, as the observed rotation was opposite what would have been expected from air jetting from beneath the retaining collar.

Tests 12 and 13, essentially repeats of Test 11, showed consistent amplitudes and directions, but only a fifth of the amplitude observed in Test 11.

Considering the possibility the flushing/cooling process might be affecting the results, the test unit was allowed to cool in a vacuum for 30 minutes prior to Test 14. The direction remained consistent with immediately previous tests, but the amplitude had dropped to a very low level.

Test 15 repeated the vacuum cooling, but for a slightly longer period. This test resulted in a noticeable oscillation of 0.75 mm, but in a direction opposite (CCW) the immediately prior tests.

Tests 16 and 17 returned to the flushing/cooling cycle. For Test 16, the resulting motion was very small, and its apparent direction of rotation was not discernable. However for Test 17, the test unit responded strongly with a 1.5 mm oscillation, back in the apparently favored CW direction.

Reviewing Tests 11 through 17, the idea of flushing with air and pumping down over consistent periods of time didn't necessarily result in consistent results.

Examination of the results of the first 17 tests reveals a surprising spread in the data. If the validation protocols had not carefully ruled out the test apparatus itself as a possible source of motion, one would be very inclined to simply attribute the observed motions to some quirk in the setup. But given the fairly rigorous testing to rule out precisely that, the results are unlikely to be caused by any "quirks". Furthermore, if some sort of systemic error in the experimental setup was causing the observed motion, it could be expected to be more consistent, and not display such actions as reversing direction and substantial changes in magnitude.

There are several plausible explanations for the odd spread in resultant motions, given the design of the test units. The units were designed to resonate around 50 KHz and also around 100 KHz. The phase relationship of those two vibratory modes should determine in what direction the predicted force would manifest itself. Unfortunately,

equipment limitations severely restricted the ability to apply precise, well-controlled signals to the test units.

Typical waveforms used are shown in Figure 13. The upper image shows a typical waveform as initially generated by the signal generator and mixer. It consists of two summed sine waves, a large amplitude wave with a frequency around 51 KHz, and a smaller amplitude wave with a frequency doubled the first of around 102 KHz, separated by a certain phase angle. Amplitude of the signal is around a volt. The lower image shows the signal as actually delivered to the PZT stack. As is apparent, it has suffered considerable degradation through the amplifier and step-up transformer. There is great rounding and attenuation of the high frequency component (and also a non-critical phase reversal of the signal). The peak to peak value of the delivered signal is just under 400 volts in this example.

Another source of signal variance has to do with the effects of beating, as previously described. Reflections at the aluminum/PZT interface cause the aluminum bar to resonant at a separate, and slightly higher frequency, than the unit as a whole. This results in interference with the primary applied signal in the test unit. The result of this interaction is difficult to predict, but it must certainly affect operation in some negative manner.

These problems suggest the level of control over the exact phase relationships of the actual standing waves, generated in the test units, was weak. If this is indeed the case, it's possible the phase relationships may have reversed from test to test (or even during a test), resulting in reversals of the observed motion. This variation in phase relationships could also explain the changes in the magnitude of the rotation.

Examination of the data shows an apparent "preference" for the torsion arm to rotate in a counterclockwise direction. But in most cases, a diminishing of the size of the rotation, then a slow increase in the new rotation direction preceded rotation reversals. This suggests possible electromechanical changes within the PZT stack, over time, possibly due to thermal effects.

Figure 14 illustrates how minor changes within a test unit may greatly affect its response. One of the test units was placed in a test stand and lightly energized with a sine wave signal as the frequency was incrementally swept from 95 KHz to 120 KHz. At each frequency step, the output of the accelerometer affixed to the end of the PZT stack was recorded. This procedure was repeated with the PZT clamping screws slightly loosened from their existing condition, then slightly tightened. Figure 13 shows that apparently minor changes in stack clamping produced substantial changes in accelerometer readings. For a given frequency, changes in accelerometer readings should be proportional to the actual acceleration changes experienced. It is apparent that at some frequencies, the change in acceleration values may change by a factor of 5. For the

frequencies in the vicinity of 102 KHz, when most of the testing took place, accelerometer readings change by a factor of three.

Minor tightening of the PZT clamping screws deliberately induced these changes. However such changes in tension may also be produced due to thermal expansion of the various components. This is particularly true for the clamping mechanism, which consists of PZTs, stainless steel screws and aluminum, each of which has differing coefficients of thermal expansion. Thus it is quite likely as the units undergo testing, thermal effects within them markedly alter their response, in manners difficult to predict.

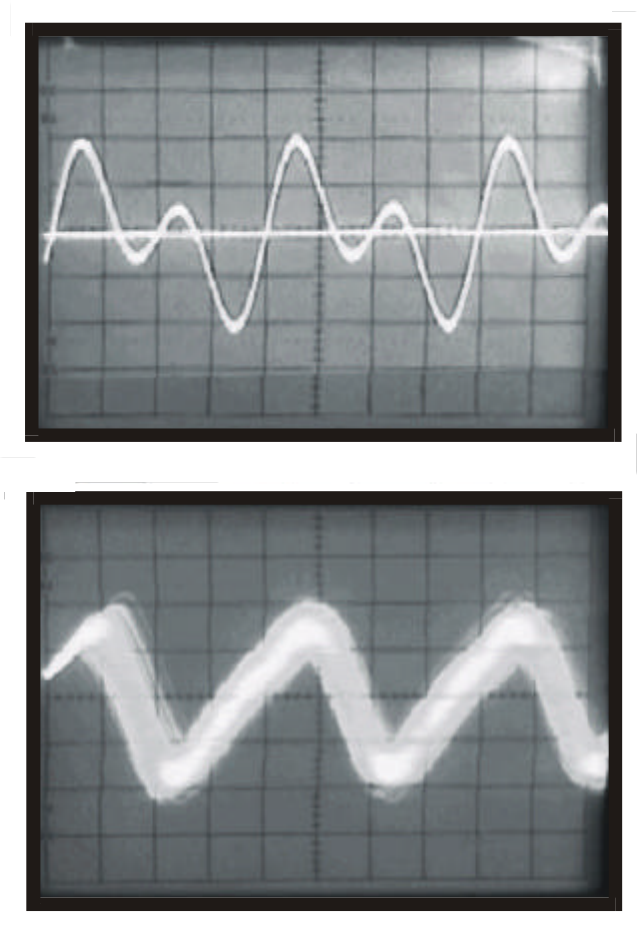

Figure 13. Oscilloscope traces showing generated versus applied signals. The upper trace shows the mixed 51/102 KHz signal as produced by the signal generator/mixer. The lower trace shows the signal as applied to the PZT stacks, after going through the amplifier and step-up transformer, and suffering serious degradation. Vertical scale on lower trace is 100 volts per graduation. The minor distortion of the scope grid is due to the image capture hardware and software used to create these images.

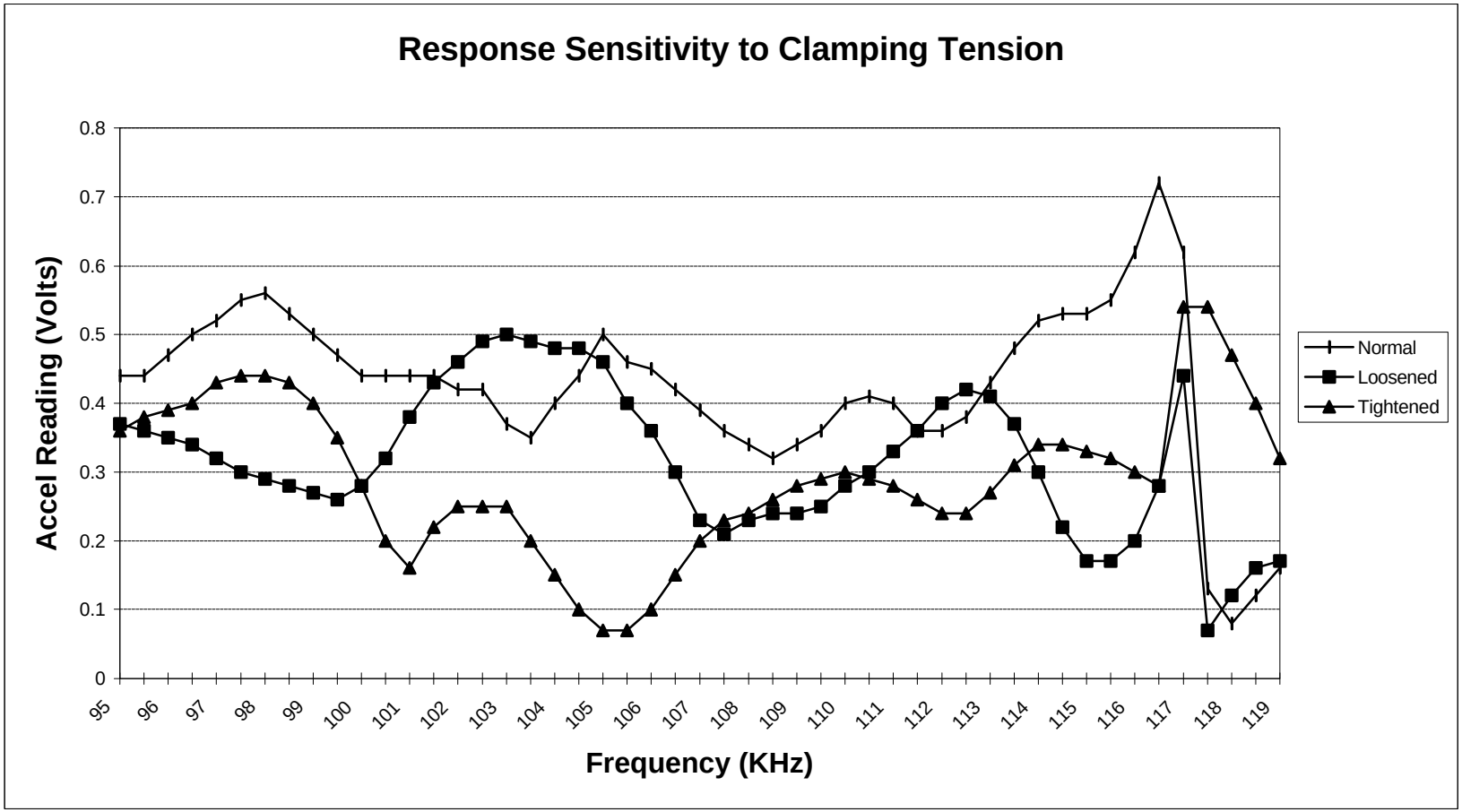

Figure 14: Response sensitivity to clamping tension. This shows the voltage values generated by the accelerometer attached to one of the unit's PZT stack over a range of frequencies with the clamping screws at their normal tension, and then loosened and tightened from that condition. The change in accelerometer voltage indications, for a given frequency, should be proportional to that actual change in acceleration.

Supplemental experiments

In view of the rather diverse results produced by the original test units, some additional tests were conducted using new units of a very different design, constructed by Dr. James Woodward.

These new devices could best be labeled “non-resonant” units, one of which is shown in Figure 15. They consisted of a stack of PZT discs 19 mm in diameter, and totaling about 16 mm in length, assembled in a manner as previously described. The PZT stack was found to longitudinally resonate at its fundamental frequency of 76 KHz. At one end of the PZT stack was a thin, aluminum retaining cap, which clamped the PZT stack onto a brass disc about 9 mm thick. Through stand testing with attached accelerometers, the brass disc was sized so as to be non-resonant at both 38 KHz and 76 KHz, the frequencies at which the PZT stack was intended to be driven. Although the PZT stack was non-resonant at 38 KHz, it was still possible to forcibly drive it at that frequency by simply subjecting the PZT discs to oscillating voltages at that frequency. The resultant response, though lower than a resonant response, was still of ample magnitude.

The primary idea behind this design was to exclude the brass portion of the test units as a possible participant of any induced mass shifts, and confine it to just the PZT stack. This was possible as the non-resonance of the brass disc prevents the longitudinal wave within the PZT stack from entering the brass disc. Ideally, the largest acoustical impedance mismatch is sought and the reaction mass would be tuned to anti-resonance. In effect, this creates an approximate fixed-free longitudinal vibratory mode within the PZT material at the 76 KHz shuttling frequency (It’s assumed the thin aluminum cap plays a negligible part), which theoretically exposes much more of the PZT material to potential acceleratory motion. The mass-shifting activity is created by the alternating polarization of the dielectric at the non-resonant 38 KHz frequency, which accelerates the ionic constituents. The relatively heavy brass disc also provides a reaction mass against which the PZT stack may act.

The supplemental series of experiments examined the behavior of these units on two different length torsion arms, as well as energizing two units at once, versus one unit. Finally, the original design test units were run again using a very short torsion arm. All data was taken using a indicator scale placed further from the test chamber (1.42 meters from the chamber axis), increasing the optical lever by three times. To directly compare the oscillation values to those of the earlier tests, the values should be divided by three. The results of this supplemental work are summarized in Tables 3 through 5.

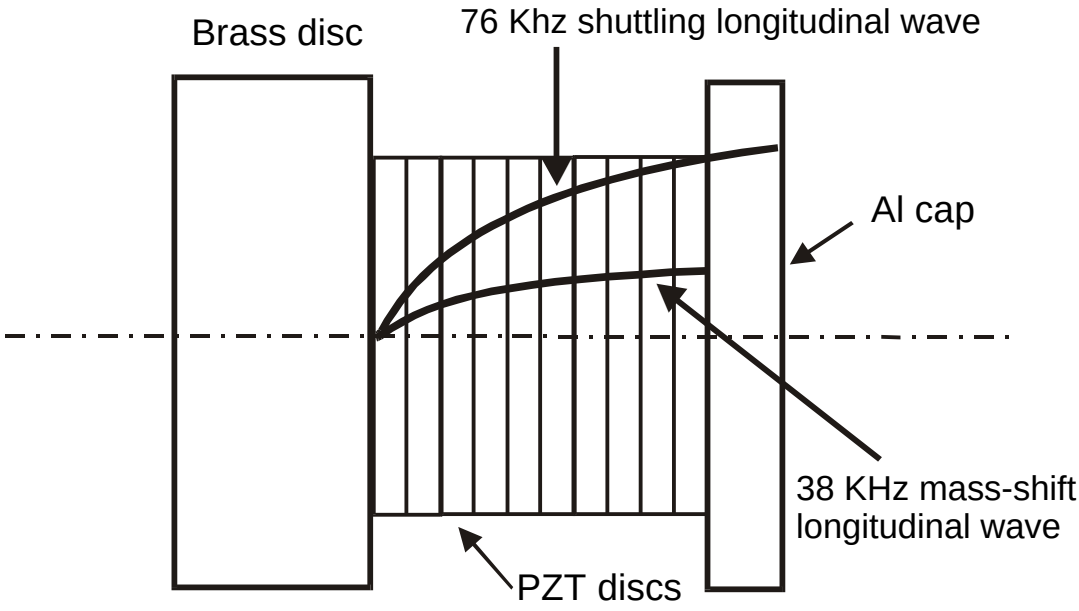

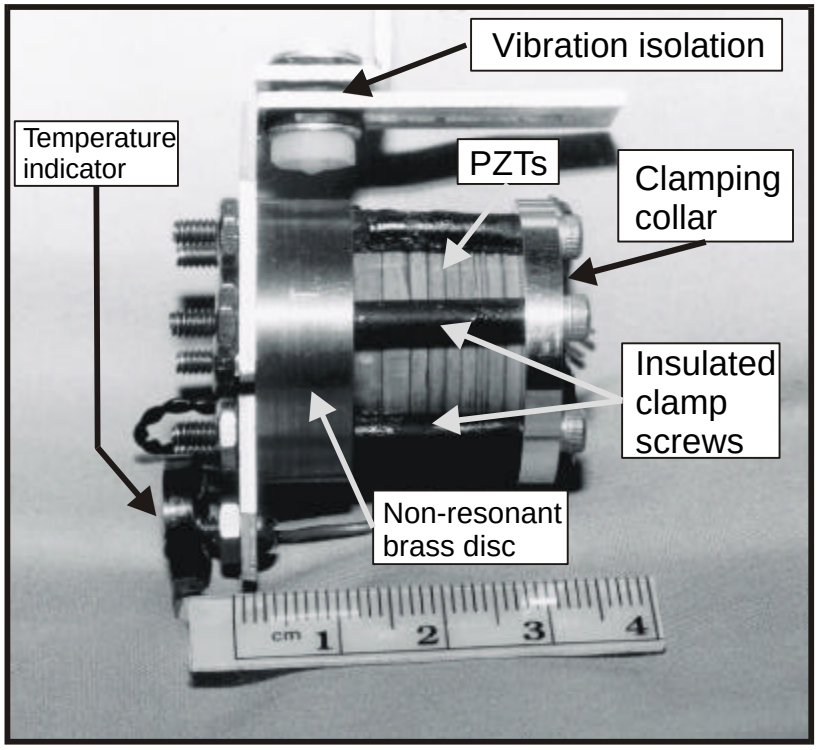

Figure 15. Non-resonant test unit details. The top cross section shows the positions of the internal longitudinal (pressure) waves within the units at 38 KHz and 76 KHz. The bottom image is a closeup view of a test unit.

Test #	Frequency (KHz)	Power (Watts)	Vacuum (microns)	Final oscillation amplitude (mm)	Force (dynes)	Notes
S1	38.5/77	104	250	8.0 CW	0.024	2 mm zero offset noted, therefore unreliable result.
S2	38.5/77	101	190	5.0 CW	0.016	
S3	38/76	103	180	4.0 CW	0.026	Oscillation was 7 mm CW after second pulse, but final pulse reduced it.
S4	38/76	106	170	2.0 CW	0.006	Signal phase reversed from S3. Pulse sequence appeared to get out of phase with oscillations.
S5	38/76	100	155	1.5 CW	0.0046	Same signal phasing as S4.
S6	38/76	100	150	1.0 CW	0.003	Signal phasing returned to that of S3.

Table 3: Test of non-resonant units on 5.16 cm arm with a period of 35 seconds. Both units on arm were energized at the same time with three, five-second pulses. All measurements were taken using the 3x optical lever scale. Divide the oscillation values by three to scale with initial experiments, r = 1.37 meters, R = 0.052 meters.

Test #	Frequency (KHz)	Power (Watts)	Vacuum (microns)	Final oscillation amplitude (mm)	Force (dynes)	Notes
S7	38/76	111	290	1.3 CW	0.003	1 mm zero offset noted.
S8	38/76	108	230	1.0 CW	0.0043	Reached maximum oscillation of 1.5 mm CW then went out of phase with automatically applied signal.
S9	38/76	119	240	2.0 CCW	0.014	Only one unit energized. Reached maximum oscillation of 2.5 mm, then went out of phase with automatically applied signal
S10	38.5/77	118	200	1.0 CCW	0.009	Only one unit energized. Reached maximum oscillation of 1.5 mm then went out of phase with automatically applied signal.
S11	38/76	119	225	2.0 CCW	0.009	Only one unit energized. Manual signal application
S12	38/76	118	190	2.0 CCW	0.009	Only one unit energized. Manual signal application.

Table 4: Test of non-resonant units on 3.0 cm arm with a period of 17.3 seconds. Both units energized for first two tests, only one unit energized in remaining 4 tests. Energization consisted of five, five-second pulses. All measurements were taken using the 3x optical lever scale. Divide the oscillation values by three to scale with initial experiments, r = 1.37 meters, R = 0.03 meters..

Test #	Frequency (KHz)	Power (Watts)	Vacuum (microns)	Final oscillation amplitude (mm)	Force (dynes)	Notes
S13	51/102	91	240	0.5 CW	0.019	Reached maximum oscillation of 2 mm after first pulse, then diminished. Manual signal application.
S14	51/102	89	200	0.5 CW	0.0027	Repeat of S13.
S15	51.5/103	91	160	6.0 CW	0.032	First test after flushing and cooling. Manual signal application.

Table 5: Tests of original units on 3.0 cm arm with a period of 15.6 seconds. Only one unit was energized with three, five-second pulses. All measurements were taken using the 3x optical lever scale. Divide the oscillation values by three to scale with initial experiments, r = 1.37 meters, R = 0.030 meters. NOTE: Orientation of test units on arm were reversed on arm from earlier testing, so instances of CW rotation would be the same as prior CCW rotation.

The first part of the supplemental testing utilized an automated method of applying the pulses, which lead to interesting results. Since the period was known to be 35 seconds, a five second pulse was applied every 30 seconds. The superficial thinking behind this procedure was that the first pulse would induce an oscillation in a particular direction, and subsequent pulses would be applied during the same portion of the torsion arm's swing, thus maximizing the cumulative effect.

The pulses during later testing were manually applied. For manual application, the initial oscillation was observed, and later pulses were manually triggered to occur at roughly the same point in the swing. No effort was made to time the manual pulse application.

Test S1 and S2 showed pronounced rotation, although Test S1 exhibited a zero offset, and therefore is less reliable than Test S2.

Test S3 initially showed a large rotation, but the final pulse in the series of three ended up reducing the oscillation. The maximum force for Test S3 was calculated on the basis of 2 pulses. Test S4 had the same parameters as Test S3, but the phasing of the two applied signals was reversed. The oscillation dropped to half that of the previous test, and the automatically applied pulses seemed to get out of phase with the motion. Test S5 was a repeat of the previous test, and the results were fairly consistent.

For Test S6, the phasing was returned to that of Test S4. Curiously, the amplitude of the oscillation failed to increase to the levels of S4, but rather continued to diminish, although the direction of rotation remained consistent.

For Tests S7 through S12, the non-resonant units were placed on a much shorter torsion arm (3.0 cm). This reduced the period from 35 seconds, in the previous tests, to 17.3 seconds. At the same time, the number of applied five-second pulses was increased from three, in the previous tests, to five.

Test S7 exhibited a fairly small rotation, and also a zero offset. This was not uncommon in the first test after reassembly of the test chamber (as a result of changing to the shorter torsion arm).

Test S8 exhibited several odd characteristics. First, it reached a maximum oscillation during the pulse application sequence that was greater then its final oscillation. That had been occasionally observed before. However, by the time the sequence of five pulses were complete, the last pulses were observed being applied almost completely out of phase with the direction of motion to which they originally gave rise. The force for Test S8 was calculated on the basis of 3 pulses, as that was the approximate point of maximum oscillation.

Test S9 continued this strange behavior where the pulses slowly went out of phase with the initially produced motion. Also the motion had reversed direction to that of a

CCW direction. There was a change in this test, as only one unit was energized, rather than the two in the previous tests. The force for Test S9 was calculated on the basis of 3 pulses, as that was the approximate point of maximum oscillation.

Tests S10 through S11 also energized only one unit. Since the previous, automatically energized tests had been producing odd results, the remaining tests were manually energized, although the computer held the length of the pulses to five seconds. Since the motion generated by the first pulse or two was rather small, it was sometimes difficult to discern when the subsequent pulses should be manually fired. As a result, Test S10 showed the applied pulses getting out of phase with the motion and force for Test S10 was calculated on the basis of 3 pulses. Tests S 11 and S12 were more successful, and all three of these tests showed definite CCW rotation.

Later analysis of the data recorded for Tests S8 and S9 revealed why the applied pulses were getting out of phase with the generated motion. As mentioned, it was naively assumed that to maximize the effect of a series of pulses, they should be applied at intervals equal to the oscillation period of the torsion arm. In fact, this is not true. If the unit under test is in actually producing a force, the oscillation period during which the force is applied will become longer than the period measured during simple harmonic motion. The motion during application of a force is not simple harmonic motion, but is in fact a driven oscillator, with very different equations of motion.

All formal tests used a pulse length of 5 seconds and usually only three of these pulses were applied in a test sequence. Given the periods involved in earlier testing, 30 to 35 seconds, three five-second pulses (of uncertain efficiency) were not enough to get seriously out of phase with the motion. However the period was then reduced, by shortening the torsion arm, to 17.3 seconds and a five second pulse became a majority proportion of the 8.7 second half period. To further exacerbate the situation, the number of pulses was increased to five. In hindsight it is obvious that such conditions must result in the applied pulses becoming out of phase with the initial motion.

This serendipitously provided a validation of the actual presence of a force. There is no plausible way for pulses applied at regular intervals, equal to the period, to become out of phase with the motion unless the period was changing. It could be argued that the passing of electric current through the suspension fiber momentarily altered the torsion constant, however validation testing showed no apparent resistive heating of the wire. If resistive heating is ruled out, the only remaining possibility for the observed phase shift is that the test units do indeed produce a small, but measurable, force.

A few final tests were done with the original resonant-design units placed on the shortened torsion arm, giving a period of 15.6 seconds. They were installed in a direction reversed from the earlier tests, so a clockwise rotation in these last tests would be the equivalent of counterclockwise rotation in the earlier tests. They were energized with the now-routine three, five-second pulses. The pulses were manually applied.

Test S13 had the somewhat unusual attribute of ending up with a final oscillation smaller than the level reached after the first pulse. Test 14 repeated the previous test, and resulted in the same final oscillation, although no interim peaks in oscillation amplitude were observed. The final test, Test S15 produced a rather sizeable oscillation. All three of these tests produced consistent, CW rotation. Given the reversely installed configuration, this observed rotation was equivalent to CCW rotation noted in earlier tests, which seems to be the "preferred direction" of these devices.

Calculation of a material constant

The derivation of the effect, contained in the Appendix, eventually leads to Eq. A.36:

$$< \mathrm{F} > = -\mathrm{f}^3 \, d l_0 \, \mathrm{P} h (2.6 \times 10^{-6}) \qquad (18)$$

Where:

$< \mathrm{F} >$: Average force in dynes.
f : Base capacitor cycling frequency in hertz.
$d l_0$: Amplitude of PZT excursion in centimeters.
P : RMS value of power delivered to capacitor in watts.
h : Empirical material constant.

This linearized approximation suggests that significant forces should be obtainable with reasonable power levels and frequencies. However the forces observed in these series of tests are very small, vastly smaller than Eq. 18 would lead one to believe. How can this be accounted for?

First of all, the derivation assumes a single particle subjected to acceleration. Since it's a single particle, all energy is assumed to go directly to acceleratory motion. When dealing with complex crystalline structures such a barium titanate, these assumptions fall a bit short. Much of the energy is in fact directed into the lattice structure itself, rather than accelerating the ions. Also, while the ions do get accelerated, different ions within each crystal get accelerated to differing degrees and in differing directions. It is therefore quite likely than Eq. 18 represents an absolute best case, and real-world results will be considerably less. But how much less?

When dealing with actual materials, it seems there should be some sort of "material constant" added to the equation (Whether it is in fact a constant still remains to be seen). This value has been given the label h for the purposes of this analysis.

To get an idea of what h must be for these tests, it is possible to calculate a value based upon empirical measurements. As the force, frequency, and power values are all known, the only remaining unknown is the excursion of the PZT stack: dl_0. Once dl_0 is known, the only remaining unknown in Eq. 18 is h.

It was possible to get a value of dl_0 during the operation of a test unit by utilizing a 633 nm He-Ne laser interferometer, as depicted in Figure 16. A small front-surface mirror was attached directly to the PZT surface of a test unit using cyanoacrylate adhesive, and the test unit mounted into the interferometer using its normal attachment points. This ensured the nature of the vibratory activity the PZTs experience will be similar to that during actual testing, as the total PZT excursion is a combination of direct, electrically stimulated oscillation, and vibration due to the resonance of the total system. The beam from the laser was split, and half the beam reflected off the mirror on the test unit. The other portion of the laser beam was reflected off a mirror mounted on a small stack of separate PZT discs. The re-combined output of the interferometer was directed onto a phototransistor detector and amplifier, which amplified and displayed a resultant voltage output on an oscilloscope.

During operation of this apparatus, the interferometer alignment was adjusted so that approximately one fringe was projected onto the detector. Next, a small 10 Hz signal, large enough to drive the interferometer output through at least one complete fringe, was applied to the PZT stack supporting the mirror, as shown on the right side of Figure 16. This provided a reference on the vertical scale of the oscilloscope, on a slow speed sweep. That is, it was possible to see precisely what constituted one fringe (or wavelength) on the vertical scale of the oscilloscope screen.

Next, the sweep speed of the oscilloscope was increased to the point where the width of the display was equal to one wavelength of the 51 KHz signal applied to the test unit. When the test unit was energized with a mixed 51/102 KHz signal, a typical image such as shown in Figure 17 was obtained. In fact, many displays were of better quality, but image capture limitations contributed some degradation.

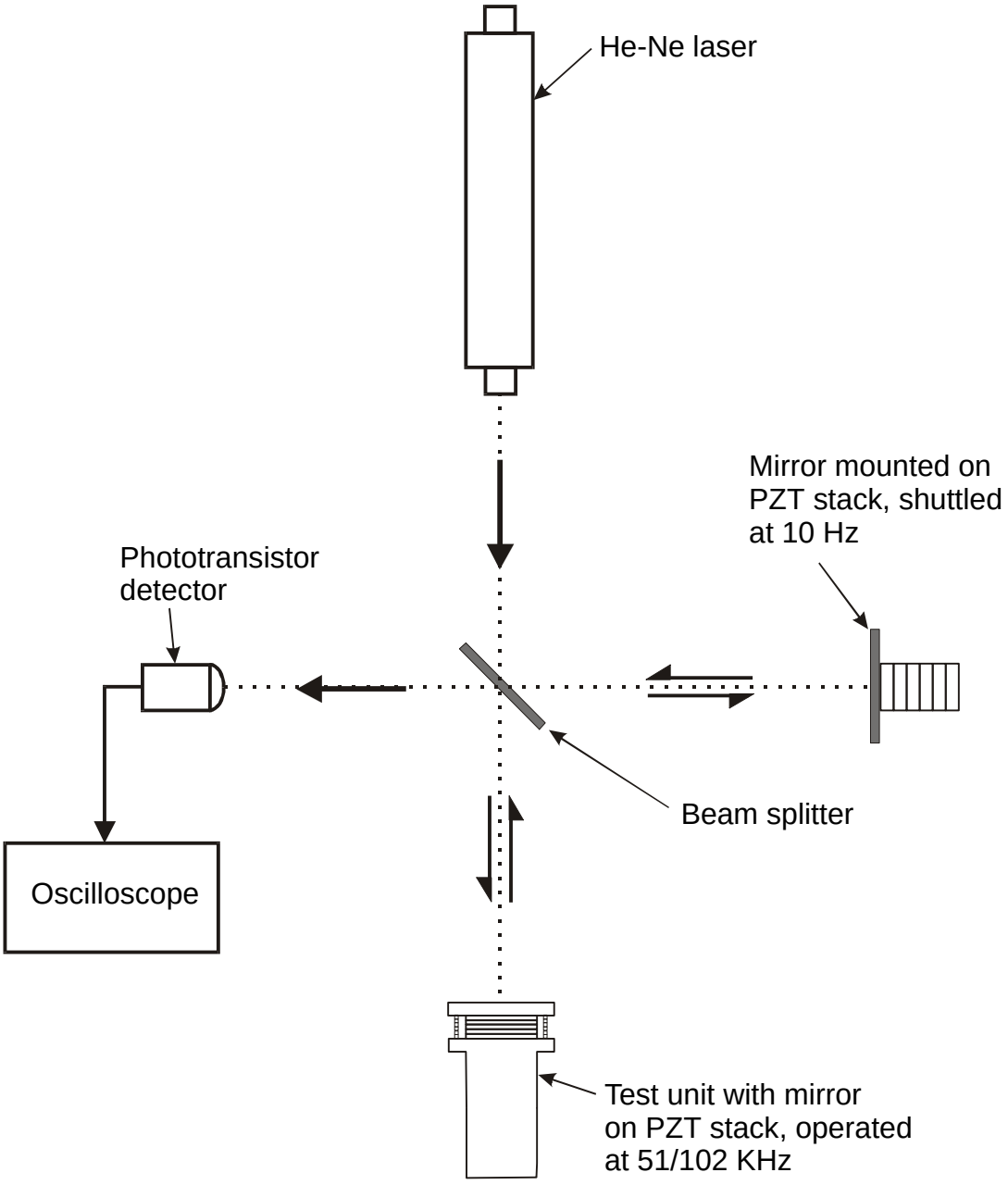

Figure 16. Laser interferometer to measure PZT excursion. The mirror on the right is shuttled at approximately 10 Hz to provide a scaling for 1 wavelength of motion on the oscilloscope. This may be then used as a reference against which the display created by the motion of the mirror on the test unit may be referenced.

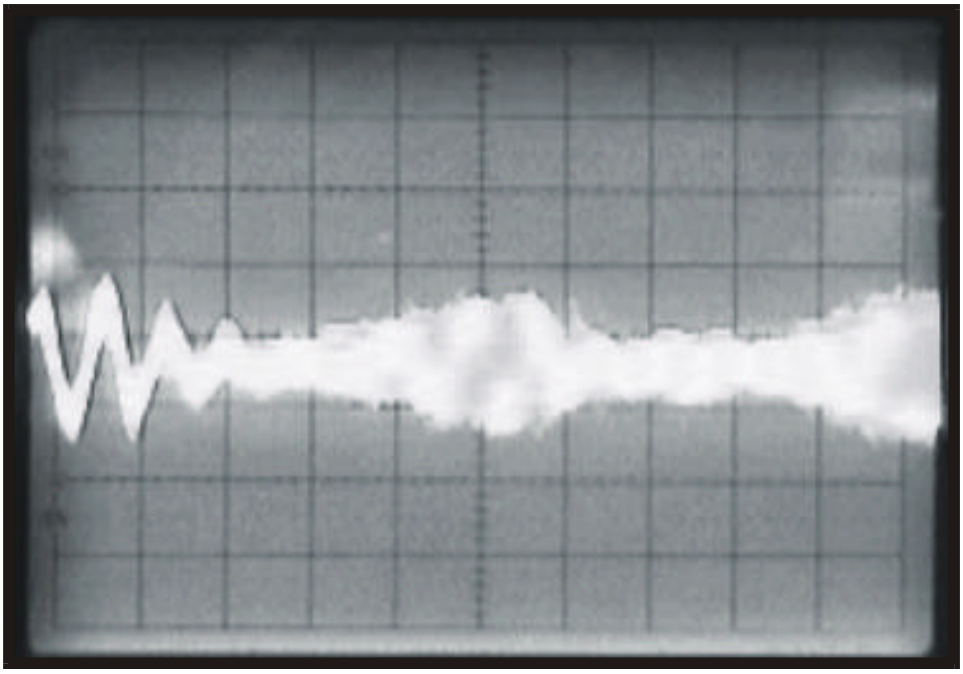

Figure 17. Oscilloscope trace of laser interferometer results. Test unit was operating at 51/102 KHz at a power level of 86 watts. The display sweep has been set so the width of the screen is equal to one wavelength at 51 KHz. One full fringe of 633 nm laser is indicated by approximately two vertical divisions. This display shows the presence of about 4 to 5 fringes.

Figure 17 shows the presence of about 4 or 5 nodes across one wavelength of the driving signal. This constitutes about 4 or 5 fringes worth of travel. With a laser wavelength of 6.33 x 10^{-7} meters, this means dl_0 is on the order of 3 x 10^{-6} meters. Using a power level of 86 watts, and the highest force obtained, 0.038 dynes, a value for h may be approximated by rearranging Eq. 18:

$$h = \frac{< \mathrm{F} >}{\mathrm{f}^3 \, dl_0 \mathrm{P} \, (2.6\times10^{-6})} \tag{19}$$

$$= \frac{0.038 \text{ dynes}}{(51\times10^{3} \text{ Hz})^3 (3\times10^{-4}\text{cm})(86 \text{ watts})(2.6\times10^{-6})}$$

$$h \approx 3\times10^{-6}$$

Since under ideal conditions, h should equal one, this seems a distressingly small value. However there is an extremely important consideration. A major assumption implicit in this is the waveform applied to the PZTs is in fact the waveform as specified in the theoretical derivation. That is, two pure sine waves, one double the frequency of the other, and offset by a certain phase lag. As mentioned, equipment limitations prevented adherence to this. This shortcoming will also act to reduce any measured effect, perhaps very significantly. Until means are available to properly drive the PZTs, this calculation of h can as best be viewed as an interim, lower boundary limit.

Changing mass-energy content as a cause of the observed force

Since the apparent measured force was so small, the question must be raised as to whether the mass shift being induced in the capacitor purely as a consequence of its changing energy density, when coupled with the piezo-induced excursion, could result in a measurable "force"?. That is, since $m = \frac{E}{c^2}$, and the energy within the capacitor is changing, is the resultant change in the capacitor's mass measurable?

Given that the energy stored in a capacitor , *U*, is equal to $\frac{CV^2}{2}$, where *C* is the capacitance and *V* is the potential across the capacitor, it is a simple matter to calculate the mass equivalent for typical tests, utilizing a voltage amplitude of 200 volts and a capacitance of 0.02 uF. Inserting this mass change for dm into Eq. A.33 of the Appendix, and using typical testing values of $dl_0 = 3\times10^{-6}$ meters , a frequency of 75 KHz, and average force, <F>, of 2.4×10^{-9} dynes is obtained. This is around 7 orders of

magnitude less than the experimentally measured values, far below the measurement threshold of the experimental apparatus. It may be reliably concluded that the changing mass-energy content of the test devices is not the source of the apparent force. Even if it were, its usefulness as a mode of propulsion would be nil, as any mass increase in one part of the system would be balanced by a mass decrease in another part of the system.

VI. Conclusions and Recommendations

This sequence of experiments strongly support the existence of some sort of very small "thrust-like" force, emanating from the test devices, causing rotation of the torsion arm. It is unlikely the observed rotations were due to building shake or other ill-defined sources of noise. The most obvious source of rotation seems to be a rather remarkable and previously unnoticed effect, caused by the vibrational activity of the test devices. Certainly the possibility still remains the rotation was caused by some overlooked, mundane source, particularly since the size of the apparent forces is so small (typically < 0.04 dynes). However the series of validation tests conducted on the apparatus and test devices seem to exclude all plausible alternative sources of motion. Essentially every possibility of motion, as dictated by conventional physics, has been excluded. Yet the torsion arm still moves, if by only a small amount.

The theory upon which these devices were designed and operated predicts the generated force to be a number of magnitudes greater than actually observed. This apparent discrepancy is likely the result of the application of less than optimum power signals (and differing from those required by theory) to the test devices, due to equipment limitations. Also there is probably some sort of material "efficiency factor" to account for energy being sunk into the piezoelectric material in modes that don't contribute to useful acceleratory motion. Initial measurements taken indicate this factor may be quite small. Finally, the precise phase relationship between the driving signal and shuttling signal has yet to be reliably determined. (For important additional possibilities also see "Author's note and addendum" in the Appendix).

In undertaking this project, a great deal was learned of the rather persnickety behavior of these devices. Perhaps most distressing was the observation that one could take reasonable care in design and implementation, yet get null results, or just as likely, false positives. Great efforts are necessary to avoid producing devices that, in effect, cancel themselves out and just sit there. There is a great deal of subtlety involved, and a careful analysis of the internal vibratory modes must be undertaken. Experimenters planning on simply attaching a capacitor to a piezoelectric crystal and vibrating it until it floats above the tabletop will be quickly disappointed. Conceptually, this is not a difficult experiment to grasp, however successful implementation lies beyond a minefield of problems.

The most serious obstacle to overcome at this point seems to be heat buildup within the test units. As presently designed, considerable power is dumped into a rather small volume of piezoelectric material, most of it eventually ending up as thermal activity.

This limits testing to fairly short bursts. The most obvious solution would appear to be increasing the operating frequency, thus decreasing the power requirements for equivalent performance. Making the units smaller, thus improving the surface area to volume ratio, would also help.

As the project progressed, a number of ideas came to light for further optimization and development of this effect. Some, such as the non-resonant design, were incorporated into the process. However time constraints eliminated a number of other, promising ideas. Some are presented here for consideration by others.

The units, as built based upon 19 mm diameter PZT discs, are far too large, resulting in rapid internal heat buildup and restrictions on operating frequencies. This appears to be a case of "smaller is better". By using PZT discs with diameters of 9 mm or less, the frequencies could be increased, yet the units still proportioned to reduce other vibratory modes. As the theory predicts the effect increases as the cube of the frequency, large gains in output may be possible. Also, smaller, thinner PZT discs reduce the operating voltage across them, and thus the power requirements, and heat dissipation.

Taking this concept to its extreme, a very promising possibility is the use of "micro-machining" to create thousands of microscopic-sized PZT stacks spread across the surface of a small silicon chip. By making the PZT layers in the stacks extremely thin, it would be possible to develop very large voltage gradients across individual layers by the application of modest voltages, perhaps on the order of tens of volts. The microscopic length of the stacks would allow for operating frequencies well into the megahertz range, perhaps higher. The surface area could also be made quite large, facilitating cooling. While the output of an individual stack would be very small, the aggregate output of thousands of such stacks, spread over a number of such chips, could be significant.

This experiment is greatly in need of being repeated using more satisfactory means of applying power signals to the PZTs. The "smoothing out" of the rather sharp initially generated signals (depicted in Figure 13) most likely severely restricted the occurrence of any possible effect. A direct-drive, high frequency, high peak current power supply seems necessary for serious further experimentation.

This experiment used a driving signal comprised of only two waveforms: a fundamental frequency intended to produce a transient mass-shift, and a signal double that of the fundamental frequency to exploit the mass-shift signal. However this doubled signal should also result in transient mass-shifts itself. To exploit these higher order mass-shifts, a third signal could be applied at four times the frequency of the fundamental signal (or double the doubled signal). This application of doubled signals, with appropriate phase relationships, could be carried out as far as one might wish, at least to practical limits. As the effect is predicted to go as the cube of the applied frequency, these higher-harmonic signals may result in quite large results.

While a torsion pendulum seems extremely well suited as a means to probe this effect further, the copper wire did not perform as well as hoped as a torsion fiber. Copper is an extremely ductile material (and fragile in the diameters used), not well suited to situations where more of a spring is required. Beryllium-copper alloys as fibers, superficially seem promising, but their electrical resistance is considerably less than copper, raising the possibility of resistive heating. The best fiber candidate located to date is a Zirconium-copper alloy. It has 92% of the electrical conductivity of copper, torsional rigidity 14% greater than copper, and 10% greater strength. Of course if downsizing can reduce power requirements of the test units, it may be possible to return to such materials as tungsten.

Appendix

Author's note and addendum:

As this thesis was being finalized, important new information was received shedding fresh light on the results of these experiments, and greatly affecting the following derivation, used as a predictor. Time constraints and the preliminary nature of the new information preclude fully incorporating it into this thesis and all of its implications have of yet not been fully worked out. Nevertheless, the new information is significant enough that it bears inclusion into this thesis, even on a tentative basis.

Under the direction of John McKeever, Oak Ridge National Laboratory (ORNL) has been independently examining the theory to determine the potential of devices such as these to actually produce a unidirectional force. John Whealton of ORNL approached the theory and derivation from a slightly different direction, and found that using sinusoidal charging and accelerating voltages, theoretically no net force would be produced, at least to low orders (McKeever 1999).

The approach Whealton used, which is in fact correct, uses the proper definition of a force as being the time derivative of the momentum, or $f = \frac{dp}{dt}$. The derivation utilized to date used what is actually an approximation, that is, force equals mass times acceleration, or $f = m\,a$ (This may be seen beginning with equation A.31 of the derivation). The differences between these two definitions of force is that in the case of a time-varying mass, the time derivative of momentum yields an additional term, which ultimately acts to cancel all (or possibly just most) of the effect predicted by the single term.

It may be more clearly seen when stated in equation form:

$$f = \frac{dp}{dt} = \frac{d(mv)}{dt} = m\frac{dv}{dt} + \frac{dm}{dt}v$$

Where p is momentum, m is the time-varying mass and v is the velocity of the mass. An f = ma approach yields only the $m\frac{dv}{dt}$ term, and Whealton showed the second term, $\frac{dm}{dt}v$, acts to exactly cancel the first term, so no net force should be expected.

This new information was conveyed to John Cramer of the University of Washington, who has been awarded a NASA Breakthrough Propulsion Physics grant to investigate the validity of this effect and to attempt a replication. Cramer utilized Mathematica to model Whealton's approach and found that any forces produced should cancel for any arbitrary periodic waveform, not merely sinusoids (Cramer 1999).

Paradoxically, it appears that this new work tends to support the experimental findings to date, rather than weaken them. For their analyses, both Cramer and Whealton used the time rate of change of the power entering and exiting a capacitor as the second derivative of the time rate of change of the energy density (as does the "traditional" derivation). However in the case of a capacitor, on a microscopic level the change in energy density is primarily kinetic. The ions in the dielectric material oscillate back and forth in response to the changing electric field. If the second time derivative of this kinetic energy density (based upon $\frac{mv^2}{2}$) is substituted into the derivation for $\frac{\partial^2 r_0}{\partial t^2}$, the equation gets considerably more complex. Specifically, a number of higher order terms are generated and it is not clear that all these higher order terms will cancel, as it appears certain non-linearities arise. As yet, the rather involved equations have not been solved exactly. However, if any terms do remain, it is likely they will be very small, in line with current experimental data. This new information is probably the best explanation as to why the observed forces are so very far below those predicted.

The problem is not with the basic mass shift. At this point there is nothing to suggest a mass shift is not occurring within the experimental devices. The problem lies in extracting a useful force out of any existent mass shift. It would seem Mother Nature views conservation of momentum as one of her primary laws, and is disinclined to let experimental "scofflaws" violate it easily. Whether small non-linearities exist which may yet be exploited in some manner is still an unanswered question, although experimental data appears promising.

The following derivation, although now shown to be overly simplified and incomplete, is included as a record of theory's understanding to date. Most of it is still valid, but the incompleteness begins at Eq. A.31, due to the flawed force representation.

Derivation of Transient Mass Fluctuations and Unidirectional Force Generation from First Principles

When an object is subjected to an acceleration, an inertial force arises acting against whatever is producing the acceleration. In Cartesian coordinates this inertial force has x, y or z components, depending upon its direction. But in relativity theory, where space is replaced by spacetime, it also has a time dimension. And when this component is included, it is known as a "four-force". To find the four-force, we begin with the general definition of force, **F,** as the derivative of momentum:

$$\mathbf{F} = -\frac{d\boldsymbol{P}}{dt} \tag{A.1}$$

where $\frac{d\boldsymbol{P}}{dt}$ is simply the proper time rate of change of four-momentum (The convention used here is that capitalized letters are 4-vectors and lowercase letters are 3-vectors).

The four-momentum, $\boldsymbol{P}$, is the four-velocity multiplied by the rest mass (and the Lorentz factor):

$$\boldsymbol{P} = g\, m_0 [\, c, v_x, v_y, v_z \,] = g\, [\, c m_0, m_0 v_x, m_0 v_y, m_0 v_z \,] \tag{A.2}$$

where m_0 is the rest mass of the object, v_x, v_y and v_z are the velocities in the various coordinate directions, and $g = \left(1 - v^2 / c^2\right)^{-1/2}$. For low, non-relativistic velocities, g may be assumed to be 1 and the "coordinate" time and proper time can be taken to be the same (since $t = g\, t$), leaving us with:

$$\boldsymbol{P} = [\, c\, m_0, m_0 v_x, m_0 v_y, m_0 v_z \,] \tag{A.3}$$

As an aside, some references use another definition of four-momentum:

$$\boldsymbol{P} = g\, [\, m_0, m_0 v_x, m_0 v_y, m_0 v_z \,] \tag{A.4}$$

In reality these apparently differing definitions are equivalent (assuming the same g factor). Eq. A.4 is expressed using what is known as “natural units”, where the velocity components are given as dimensionless fractions (≤ 1) of the speed of light, and *c* itself represented as unity. For the purposes at hand here, Eq. A.3, which expresses momentum in normal mks units, is somewhat preferable, so we will proceed with that representation:

$$\boldsymbol{P} = [c\,m_0, m_0 v_x, m_0 v_y, m_0 v_z] \tag{A.5}$$

Since the four-force is the (proper) time derivative of the four momentum,

$$\mathbf{F} = -\frac{\partial \boldsymbol{P}}{\partial t} = -[\frac{\partial}{\partial t}(c\,m_0), \frac{\partial \boldsymbol{p}}{\partial t}] \tag{A.6}$$

or, using **f** to represent the "three-force" and since $\frac{\partial c}{\partial t} = 0$,

$$\mathbf{F} = -\left[c\frac{\partial m_0}{\partial t}, \mathbf{f} \right] \tag{A.7}$$

The derivation to this point is contained and clearly explained in detail in *Introduction to Special Relativity*, by Rindler (1991) Section 35. The use of m_0 is adequate when considering a point mass, but when talking of anything of any size, m_0 must be replaced with the proper density, r_0. Further, the inertial field is a "force per unit mass", so we need to also divide Eq. A.7 by the object's mass to normalize it, or in the case we now have, r_0, so Eq. A.7 now becomes:

$$\mathsf{F} = -\left[\frac{c}{r_0}\frac{\partial r_0}{\partial t}, \boldsymbol{f} \right] \tag{A.8}$$

where F and $\boldsymbol{f}$ are now field strengths (where $\boldsymbol{f} = \frac{\mathbf{f}}{r_o}$). But: $r_0 = \frac{e_0}{c^2}$, where e_0 is the rest mass energy density, so:

$$\mathsf{F} = -\left[\frac{1}{r_0 c}\frac{\partial e_0}{\partial t}, \boldsymbol{f} \right] \tag{A.9}$$

We next take the four divergence of the field, $\left(\frac{1}{c}\frac{\partial \mathsf{F}_t}{\partial t} + \frac{\partial \mathsf{F}_x}{\partial x} + \frac{\partial \mathsf{F}_y}{\partial y} + \frac{\partial \mathsf{F}_z}{\partial z} \right)$ and set it equal to the proper source charge density, which is equal to Gr_0, where G is the Newtonian constant of gravitation. This is simply Gauss's Law extended into four dimensions:

$$\nabla_4 \cdot \mathsf{F} = -\frac{1}{c}\frac{\partial}{\partial t}\left(\frac{1}{r_0 c}\frac{\partial e_0}{\partial t} \right) - \nabla \cdot \boldsymbol{f} = 4\pi G r_0 \tag{A.10}$$

$$-\frac{1}{r_0 c^2}\frac{\partial^2 e_0}{\partial t^2} + \frac{1}{r_0^2 c^2}\frac{\partial e_0}{\partial t}\frac{\partial r_0}{\partial t} - \nabla \cdot \boldsymbol{f} = 4\pi G r_0 \tag{A.11}$$

But again, $r_0 = \frac{e_0}{c^2}$, so

$$-\frac{1}{r_0 c^2}\frac{\partial^2 e_0}{\partial t^2} + \frac{1}{r_0^2 c^4}\left(\frac{\partial e_0}{\partial t}\right)^2 - \nabla \cdot \boldsymbol{f} = 4\pi G r_0 \tag{A.12}$$

$$-\frac{1}{r_0 c^2}\frac{\partial^2 e_0}{\partial t^2} + \left(\frac{1}{r_0 c^2}\right)^2\left(\frac{\partial e_0}{\partial t}\right)^2 - \nabla \cdot \boldsymbol{f} = 4\pi G r_0 \tag{A.13}$$

Holding Mach's Principle to be correct, we assume the rest energy of a mass is equal to its proper density times the gravitational potential due to all the matter in the universe, f, experienced by the mass:

$$e_0 = r_0 f \tag{A.14}$$

We'll now expand and simplify the first two terms of Eq. A.13 into a more useful form. Starting with the first term:

$$-\frac{1}{r_0 c^2}\frac{\partial^2 e_0}{\partial t^2} = -\frac{1}{r_0 c^2}\frac{\partial^2 (r_0 f)}{\partial t^2}$$

$$= -\frac{1}{c^2}\frac{\partial^2 f}{\partial t^2} - \frac{2}{r_0 c^2}\frac{\partial f}{\partial t}\frac{\partial r_0}{\partial t} - \frac{f}{r_0 c^2}\frac{\partial^2 r_0}{\partial t^2} \tag{A.15}$$

Next, expanding and simplifying the second term of Eq. A.13:

$$\left(\frac{1}{r_0 c^2}\right)^2\left(\frac{\partial e_0}{\partial t}\right)^2 = \frac{1}{c^4}\left(\frac{\partial f}{\partial t}\right)^2 + \frac{2f}{r_0 c^4}\frac{\partial r_0}{\partial t}\frac{\partial f}{\partial t} + \left(\frac{f}{r_0 c^2}\right)^2\left(\frac{\partial r_0}{\partial t}\right)^2 \tag{A.16}$$

Combining the expanded first and second terms (Eqs. A.15 and A.16) and substituting back into Eq. A.13 gives:

$$-\frac{1}{c^2}\frac{\partial^2 f}{\partial t^2} - \frac{2}{r_0 c^2}\frac{\partial f}{\partial t}\frac{\partial r_0}{\partial t} - \frac{f}{r_0 c^2}\frac{\partial^2 r_0}{\partial t^2} + \frac{1}{c^4}\left(\frac{\partial f}{\partial t}\right)^2 + \frac{2f}{r_0 c^4}\frac{\partial r_0}{\partial t}\frac{\partial f}{\partial t} + \left(\frac{f}{r_0 c^2}\right)^2\left(\frac{\partial r_0}{\partial t}\right)^2 - \nabla \cdot \boldsymbol{f} = 4\pi G r_0$$

Per Sciama (1953), the gravitational potential should be : $f = c^2$, then $\frac{2f}{r_0 c^4} = \frac{2}{r_0 c^2}$, so the second and fifth terms cancel, leaving:

$$-\frac{1}{c^2}\frac{\partial^2 f}{\partial t^2} - \frac{f}{r_0 c^2}\frac{\partial^2 r_0}{\partial t^2} + \frac{1}{c^4}\left(\frac{\partial f}{\partial t}\right)^2 + \left(\frac{f}{r_0 c^2}\right)\left(\frac{\partial r_0}{\partial t}\right)^2 - \nabla \cdot \boldsymbol{f} = 4\pi G r_0 \qquad \text{(A.17)}$$

Since the field is irrotational, the three-vector force, $\boldsymbol{f}$, may be defined as $-\nabla f$. So:

$$-\nabla \cdot \boldsymbol{f} = \nabla^2 f \qquad \text{(A.18)}$$

Substituting this back into the previous equation and rearranging gives a basic field equation:

$$\nabla^2 f - \frac{1}{c^2}\frac{\partial^2 f}{\partial t^2} = 4\pi G r_0 + \frac{f}{r_0 c^2}\frac{\partial^2 r_0}{\partial t^2} - \frac{1}{c^4}\left(\frac{\partial f}{\partial t}\right)^2 - \left(\frac{f}{r_0 c^2}\right)^2\left(\frac{\partial r_0}{\partial t}\right)^2 \qquad \text{(A.19)}$$

The left hand side of the equation is the d'Alembertian ( ) of f. The d'Alembertian is a relativistically invariant four-dimensional wave operator, valid in any Lorentz frame. The first term on the right hand side is the standard Newtonian gravitational source term, but three interesting periodic, time-varying terms (time-varying because they vary with respect to the first or second derivative of time) have now appeared.

The third term on the right hand side contains a factor of $1/c^4$, as well as being the time rate of change of the gravitational potential. As the gravitational potential is not likely to change much with time (it's a quasi-steady-state condition), the term at most will be exceedingly small and may be ignored.

The last term on the right hand side also has a factor of $1/c^4$, but it also has the square of the change in proper mass density with respect to time. If this term becomes large enough (from perhaps extremely rapid shifts per time), it has the potential to affect the value of the equation. It's also interesting to note that this term is always negative. If this term gets large enough, it can take the entire result negative. For now we will assume it also is small enough not to affect the overall value of the equation and may be ignored. The approximated equation now becomes:

$$\nabla^2 f - \frac{1}{c^2}\frac{\partial^2 f}{\partial t^2} \approx 4\pi G r_0 + \frac{f}{r_0 c^2}\frac{\partial^2 r_0}{\partial t^2} \qquad \text{(A.20)}$$

Factoring out $4\pi G$ on the right hand side gives:

$$\nabla^2 f - \frac{1}{c^2}\frac{\partial^2 f}{\partial t^2} \approx 4\pi G\left(r_0 + \frac{f}{4\pi G r_0 c^2}\frac{\partial^2 r_0}{\partial t^2}\right) \qquad \text{(A.21)}$$

Presented in this way, it becomes apparent that the time-varying term is an "adjustment" to the proper mass density of the source, based upon the time rate of change in the object's proper density, which is either added to or subtracted from the proper density depending upon the instantaneous value of the second time derivative. Note also that while this is a linear equation in f, the term containing r_0 is non-linear, with r_0 appearing in the derivative and the denominator. Focusing on this term, the change in the overall proper mass density is then simply:

$$dr_0 = \frac{f}{4p G r_0 c^2} \frac{\partial^2 r_0}{\partial t^2} \tag{A.22}$$

Now consider a capacitor to which a sinusoidal voltage is applied. The proper density, r_0 of the capacitor's dielectric material is E_0 / c^2, where E_0 is the instantaneous proper energy density. But the first partial derivative of E_0 with respect to time, integrated over the volume of the capacitor's dielectric is the instantaneous power P_i being delivered to the capacitor. So the equation may be rewritten to give the change in mass of the capacitor as:

$$d m_{cap} \approx \frac{f}{4p G r_0 c^4} \frac{d P_i}{dt} \tag{A.23}$$

The instantaneous power, P_i, applied to a capacitor is the product of the instantaneous voltage $[V=V_0 \, sin(wt)]$, and the instantaneous current $[I=I_0 sin(wt+a)]$, where a is the phase angle between the voltage and current, which is $+p/2$ for capacitors. Then P_i becomes:

$$P_i = V_0 I_0 \, sin(wt) \, sin(wt+a) \tag{A.24}$$

Differentiating P_i gives:

$$\frac{d P_i}{dt} = V_0 I_0 w[cos(wt) \, sin(wt+a) + sin(wt) cos(wt+a)] \tag{A.25}$$

and by rearranging and using various trigonometric identities:

$$\frac{d P_i}{dt} = V_0 I_0 w[sina \; cos(2wt) + sin(2wt) \, cosa] \tag{A.26}$$

Finally, substituting $+p/2$ for a gives:

$$\frac{d P_i}{dt} = V_0 I_0 w \, cos(2wt) = 2P w \, cos(2wt) \tag{A.27}$$

where P is the RMS power ($P = V_0 I_0 / 2$). Using Sciama's earlier assumption of $f = c^2$, we set $f / c^2 = b \approx 1$, and substitute back into Eq. A.23 to get:

$$d m_{cap} \approx \frac{\mathrm{P} b w}{2p G r_0 c^2} cos(2wt) \tag{A.28}$$

The amplitude of the mass shift, $d m_0$, can be defined as:

$$d m_0 = \frac{\mathrm{P} b w}{2p G r_0 c^2} \tag{A.29}$$

and the time varying mass shift can be simply written as:

$$d m_{cap} \approx d m_0 \, cos(2wt) \tag{A.30}$$

A transiently varying shift in the mass of the dielectric of a capacitor, while interesting, is not immediately useful. However, when coupled to a piezoelectric transducer, oscillating at the same frequency as the mass shift (which is twice the cycling rate of the capacitor), a constant, unidirectional force may be produced.

Consider a massless piezoelectric transducer (PZT), to which a capacitor undergoing a transient mass shift is affixed. The PZT is driven at the same frequency $(2w)$ as the mass shifts, but with some phase offset, g . The sinusoidal signal creates a time varying change in the length of the PZT of amplitude $d l_0$.

The position of the face of the PZT at any given point in time is $d l_0 \, cos(2wt + g)$, if the other face is attached to a massive block.

Therefore, the velocity of the face of the PZT, $\mathbf{v} = -2wd l_0 \, sin(2wt + g)$,
and the acceleration of the face of the PZT, $\mathbf{a} = -4w^2 d l_0 \, cos(2wt + g)$.

The total mass of the capacitor consists of its basic rest mass, m_0, plus its time varying mass shift, $d m_0 \, cos(2wt)$. If this combination of PZT and capacitor is placed against a relatively massive body, the body will experience a reaction force **F**, equal to the mass of the capacitor times the acceleration imparted to it by the PZT (**F** = ma). This may be written as:

$$\mathbf{F} = [m_0 + d m_0 \, cos(2wt)]\left[-4w^2 d l_0 \, cos(2wt + g)\right]$$

or, multiplying out,

$$\mathbf{F} = -m_0 4w^2 d\, l_0 \cos(2wt+g) - 4w^2 d\, l_0 \cos(2wt+g) d\, m_0 \cos(2wt) \qquad \text{(A.31)}$$

The first term will simply time average to zero over any whole number of cycles, producing no net effect, and may be discarded. However the second term ends up producing a constant average force, <F>, for a given phase offset g . The sequence of trigonometric steps is as follows:

$$\begin{aligned} -4w^2 d\, l_0 \cos(2wt+g) d\, m_0 \cos(2wt) &= -4w^2 d\, l_0 d\, m_0 \cos(2wt)[\cos(2wt)\cos g - \sin(2wt)\sin g] \\ &= -4w^2 d\, l_0 d\, m_0 \left[\frac{1}{2}\cos(g) + \frac{1}{2}\cos(4wt+g)\right] \\ &= -2w^2 d\, l_0 d\, m_0 \cos(g) - 2w^2 d\, l_0 d\, m_0 \cos(4wt+g) \end{aligned} \qquad \text{(A.32)}$$

Note that the second term time averages to zero. This leaves only the first term, a constant value, dependent upon g . $Cos(g)$ reaches a maximum of 1 when the phase offset between the capacitor oscillation and the PZT oscillation is equal to 0. This gives a time-averaged force of:

$$< \mathrm{F} > = -2w^2 d\, l_0 d\, m_0 \qquad \text{(A.33)}$$

Assuming $b \approx 1$ and substituting back in for $d\, m_0$ (Eq. A.31) gives:

$$< \mathrm{F} > = -\frac{w^3 d\, l_0 \mathrm{P}}{p G r_0 c^2} \qquad \text{(A.34)}$$

Eq. A.34 is adequate when considering an infinitesimal capacitor, subjected to an ideal charging cycle. Unfortunately, real-world material considerations are less cooperative. This derivation assumes all energy put into the system goes directly to acceleratory motion of the dielectric material. When dealing with complex crystalline structures such as typical capacitor dielectrics, this assumption is less than accurate. Much of the energy is in fact directed into the lattice structure itself, rather than accelerating the ions. Also, while the ions do get accelerated, different ions within each crystal get accelerated to differing degrees and in differing directions. Therefore Eq. A.34 represents an absolute best case, and real-world results will be considerably less.

To adjust for this, an empirically determined material constant (or "efficiency factor) is introduced, denoted as h . Under ideal conditions, $h = 1$, however preliminary experiments have suggested h is far smaller than 1. (Note that the value of h could have been incorporated into the previously used constant b , but for clarity in this derivation b will remain exclusively a gauge of gravitational potential and h will pertain strictly to dielectric material issues).

Adding h to Eq. A.34 gives:

$$< \mathrm{F} > = -h \frac{w^3 d\, l_0 \mathrm{P}}{p\, G\, r_0 c^2} \tag{A.35}$$

Substituting for the constants, using a value of $5\ \mathrm{gm/cm^3}$ for r_0 (typical value for capacitor dielectrics), and factoring to accommodate more useful variables:

$$< \mathrm{F} > = -\mathrm{f}^3\, d\, l_0\, \mathrm{P} h\, (2.6 \times 10^{-6}) \tag{A.36}$$

Where:

$< \mathrm{F} >$: Average force in dynes.
f : Base capacitor cycling frequency in hertz.
$d\, l_0$: Amplitude of PZT excursion in centimeters.
P : RMS value of power delivered to capacitor in watts.
h : Empirical material constant.

Until h can be accurately determined, caution is urged in the use of this final equation as any sort of a force predictor. It should be noted this equation is the end result of a linear approximation of a non-linear equation, and as such may give increasingly inaccurate predictions as more extreme input values are used.

Reference List

Cramer, John G. 1999. Electronic communication to J.F. Woodward, 28 October, 1999.

EDO Ceramics. 1998. *Piezoelectric ceramics: Material Specifications – Typical Applications*. Salt Lake City: EDO Ceramics.

Frederick, Julian R. 1965. *Ultrasonic Engineering*. New York: John Wiley & Sons.

Harker, Ralph J., 1983. *Generalized Methods of Vibration Analysis*. New York: John Wiley & Sons.

McKeever, John W. 1999. Electronic communication, 19 October, 1999.

Moulson, A. J., and Herbert, J. M. 1990. *Electroceramics*. New York: Chapman and Hall.

Rindler, Wolfgang. 1991. *Introduction to Special Relativity, 2nd Edition*. New York: Oxford University Press.

Sciama, D. W. 1953. *Monthly Notes of the Royal Astronomical Society*, no. 113:34-42.

Talley, R. L. 1991. *Twenty First Century Propulsion Concept*. NTIS, AD-A237 853/7INZ.

Woodward, J.F. 1991. Measurements of a Machian transient mass fluctuation. *Foundations of Physics Letters*, no. 4:407-423.

Woodward, J.F. 1992. A stationary apparent weight shift from a transient Machian mass fluctuation. *Foundations of Physics Letters*, no. 5:425-442.

Woodward, J.F. 1996. A laboratory test of Mach's Principle and strong-field relativistic gravity. *Foundations of Physics Letters*, no. 9:247-293.

Woodward, J.F. 1997. Twists of fate: Can we make traversable wormholes in spacetime? *Foundations of Physics Letters*, no. 10:153-181.

Woodward, J.F. and Mahood, T. 1999. What is the cause of inertia? *Foundations of Physics*, no. 29:899-930.